Chapter 4

Terahertz Wave Conversion from Linear to Circular Polarization by Graphene Metasurface Featuring Ultrawideband Tunability

4.1. Introduction

Metasurface-based circular polarization (CP) converters have been preferred owing to their compact configuration and low atmospheric attenuation [321]-[322]. Graphene has been integrated with the metasurface design to offer tunability in the terahertz-gap applications due to its high electrical conductivity, improved optoelectronic properties, remarkable mechanical properties, and durability [160]. A multilayered graphene-based structure and a graphene-metal hybrid metasurface [323]-[324] have been explored in lower terahertz region, but their practical implementations seem to be difficult. Metasurface configurations with graphene structures on the substrates [325]-[326] have also been examined for CP conversion of the incident EM wave; nevertheless, the fractional 3-dB axial ratio bandwidth achieved by them is quite narrow. The CP conversion performances in those devices have been found to be angularly unstable too.

The present work addresses all the important aspects, which are mostly uncommon altogether in the previous designs, to be an improved and competent candidate. The proposed design is much simpler in terms of the deposition of the graphene layer on the top surface of the gold-backed silicon dioxide (SiO_2) substrate. It also provides a moderate 3-dB fractional axial ratio

bandwidth (FARBW) of 46.15%; significantly improved from the existing ones [323], [325], [327]. The configuration further maintains the effective homogeneity limit in the sub-wavelength domain. The proposed reflective-type linear to circular polarization converter (RLCPC) shows a more stable CP conversion under different incident angles than those in [323]-[327] as it demonstrates angular stability up to 40° for both TE and TM polarizations. Thus, the structure is beneficial for the THz beam scanning antennas by providing a wider angular steering range. The CP performances of the proposed structure have been compared with the existing ones as shown in Table 4.1. Due to the scarcity of the available experimental setup towards the fabrication and measurement of the proposed device in our country, a detailed circuit model for the designed RLCPC has been designed to validate the EM simulated performances. The values of all the circuit components have been elaborately derived and documented. The proposed graphene metasurface also has an advantage over the existing ones in terms of the electrical biasing set-up due to its continuous spanning on the SiO_2 substrate. The biasing set-up can be established easily between the top continuous graphene metasurface and the bottom gold layer by using a single variable DC biasing. The proposed metasurface can be integrated with THz antenna to achieve an easy switching of polarization states between uplinking and downlinking for wireless communication in space applications, military radar applications, RCS reduction [328]-[329], etc.

4.2. Design and Simulated Outcomes

A. Design and working mechanism of the Structure

The proposed prototype consists of three layers. Two differently shaped and perpendicularly arranged thin elliptical slots are generated from a 1 nm thick graphene layer deposited on top of a completely gold-backed silicon dioxide (t =12 μm) substrate with a dielectric constant of

Table 4.1. Comparison with Existing Graphene-based Metasurface LP to CP Converter

Graphene-based polarization converters	Configuration	3-dB FARBW (%)	Thickness	Size of lattice	Angular stability ($\theta°$)
[323]	Graphene-silicon-7-layer graphene	20.22%	$\lambda_o/12.49$	$\lambda_o/9.37$	NA
[324]	Graphene-Metal-hybrid metasurface-SiO_2-Neltec NY9208-Metal	84.86%	$\lambda_o/10.89$	$\lambda_o/4.46$	NA
[325]	Graphene-silicon-metal	9%	$\lambda_o/11.54$	$\lambda_o/5.92\times\lambda_o/7.57$	Up to 20°
[326]	Metal-graphene-hybrid metasurface-SiO_2-graphene-dielectriic-metal	18.18%	$\lambda_o/9.91$	$\lambda_o/4.99$	NA
[327]	Graphene metasurface-SiO_2-graphene	1.11% 2.22%	$\lambda_o/7.89$	$\lambda_o/10.70$	NA
Proposed structure	Graphene metasurface-SiO_2-metal	46.15%	$\lambda_o/7.69$	$\lambda_o/8.33$	Up to 40°

3.9 (ϵ_{SiO_2}) and a loss tangent of 0.001. Silicon dioxide (SiO_2) is dispersive in terahertz (THz) frequency region. Therefore, SiO_2 has been selected as the substrate material by incorporating the inherent treatment protocol for SiO_2 in CST Microwave Studio 2017 in favour of Debye model [226], [330]-[333]. All the dimensions of the meta-atom are described in the caption of Fig.

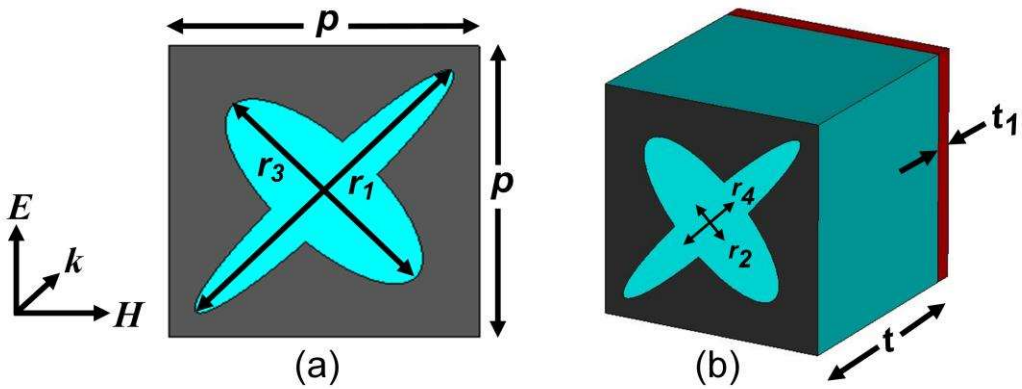

Fig. 4.1. (a) Top view, and (b) perspective view of the wideband graphene-based metasurface (RLCPC) for linear to circular polarization conversion in lower MIR region (r_1 = 7 µm, r_2 = 1 µm, r_3 = 5 µm, r_4 = 2 µm, p = 12 µm, t = 12 µm, t_1 = 1 µm).

4.1. The graphene layer of the design has the following properties: thickness of graphene layer t_g = 1 nm, chemical potential μ_c = 1 eV and relaxation time τ = 1 ps. The thickness (t_1) of the bottom gold layer ($\sigma_{elect.} = 4.56\times10^7$ S/m) is chosen as 1 μm. The whole structural configuration has been electromagnetically investigated by using a conclusive set of data obtained from [226]. The properties of various materials used in the design is listed in Table 4.1.

The physical realization of the proposed device can be done using graphene deposition on a gold backed silicon dioxide (SiO_2) substrate. The deposition of graphene via physical deposition process is not possible, however, graphene can be deposited via chemical vapor deposition process (CVD) [97]-[99]. The major radii (r_1 and r_3) and minor radii (r_2 and r_4) of the two elliptical slots are optimized to achieve control over the reflection magnitudes and phases for two orthogonal linearly- polarized (LP) wave components [328].

A *y*-polarized LP wave is incident on the top face of the proposed metasurface and the reflected wave is CP in nature. The magnitude and phase of the wave reflected from the proposed metasurface have been controlled via subwavelength dimensions of the meta-atoms [334]. The above said fact can be verified from the extraction of the primary parameters *viz.*, magnitude and phase responses of the co- and cross-polarized reflection coefficients (R_{yy} and R_{xy}) followed by required calculations using Stokes' relations [335]. Since graphene's Fermi level (E_f) plays the key role in graphene's spatial conductivity, graphene's fermi level can be tuned by various techniques, including impurity doping, mechanical straining, as well as DC biasing as reported previously [97]-[99].

$$\boldsymbol{E_y} = \boldsymbol{y}E_0 e^{jk_z z} = \boldsymbol{E}_{yE_1} + \boldsymbol{E}_{yE_2}$$

$$\boldsymbol{E_y} = \left[\frac{\sqrt{2}}{2}\right]\left[\boldsymbol{e_1}E_0 e^{jk_z z} + \boldsymbol{e_2}E_0 e^{jk_z z}\right] \quad (4.1)$$

The working mechanism of the proposed RLCPC can be explained elaborately by resolving the incident *y*-polarized EM wave E_y into two perpendicular E-field vectors $\boldsymbol{E}_{yE_1}$ and $\boldsymbol{E}_{yE_2}$ as shown in equation (4.1), where $\boldsymbol{E}_{yE_1}$ makes an angle of φ with $\boldsymbol{E}_y$. $\boldsymbol{E}_{yE_1}$ is parallel to the larger elliptical slot while $\boldsymbol{E}_{yE_2}$ is oriented along shorter elliptical slot as shown in Fig. 4.2. After interacting with the top graphene metasurface, the incident wave enters into the substrate and undergoes multiple reflections [336]-[337]. The incident *y*-polarized wave $\boldsymbol{E_y}$ can be expressed as given in equation (4.1). Here, $\boldsymbol{e_1}$ and $\boldsymbol{e_2}$ are the unit vectors along the directions

$$\boldsymbol{E_{ryE_2}} = \boldsymbol{E_{yE_2}}\boldsymbol{r_{yE_2}}\boldsymbol{e^{i\varphi_{yE_2}}} \qquad \boldsymbol{E_{ryE_1}} = \boldsymbol{E_{yE_1}}\boldsymbol{r_{yE_1}}\boldsymbol{e^{i\varphi_{yE_1}}}$$

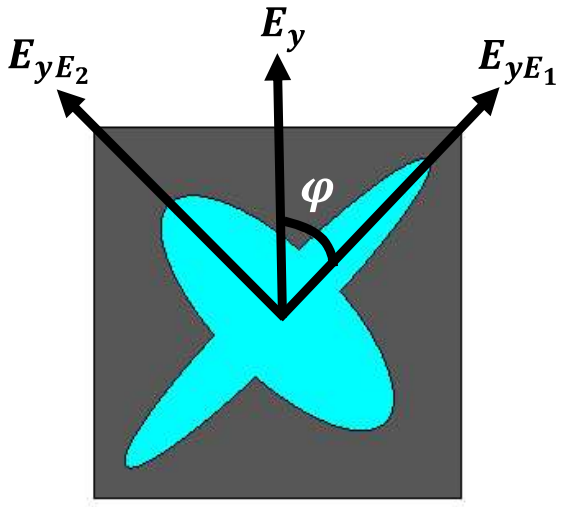

Fig. 4.2. Incident vertically polarized EM wave (E_y) is decomposed into two components E_{yE_1} and E_{yE_2}.

of $\boldsymbol{E}_{yE_1}$ and $\boldsymbol{E}_{yE_2}$, k_z is the light propagation vector along *z*-axis and the bold letters are denoted as vector components. The reflected co-efficients along the directions of $\boldsymbol{E}_{yE_1}$ and $\boldsymbol{E}_{yE_2}$ vectors are $r_{yE_1}e^{j\varphi_{yE_1}}$ and $r_{yE_2}e^{j\varphi_{yE_2}}$, respectively. Accordingly, the reflected wave can be presented as given in equation (4.2).

$$\boldsymbol{E_r} = \left[\frac{\sqrt{2}}{2}\right]\left[\boldsymbol{e_1}r_{yE_1}E_0e^{j(k_zz+\varphi_{yE_1})} + \boldsymbol{e_2}r_{yE_2}E_0e^{j(k_zz+\varphi_{yE_2})}\right] \quad (4.2)$$

Circular polarization can be realized when $|r_{yE_1}| = |r_{yE_2}|$ and $|\varphi_{yE_1} - \varphi_{yE_2}| = \Delta\phi = 90^{\circ}$ or an odd multiple of 90° have been satisfied simultaneously. The equation (2) can be accordingly re-written as equation (4.3) [334].

$$\boldsymbol{E_r} = \left[\frac{\sqrt{2}}{2}\right] E_0 \left[\boldsymbol{e_1} e^{j(k_z z + \varphi_{yE_2} + 90^{\circ})} + \boldsymbol{e_2} e^{j(k_z z + \varphi_{yE_2})}\right] \quad (4.3)$$

The proposed graphene-based reflective metasurface produces a conversion of a linearly *y*-polarized wave into its circular polarized form with the validation of the aforementioned theory.

B. Simulated Results

This section demonstrates the EM simulation results and the calculations of Stokes' parameters. The proposed device is working as a linear to circular polarization converter in between 3.75 THz and 6 THz. The main reason for this conversion is

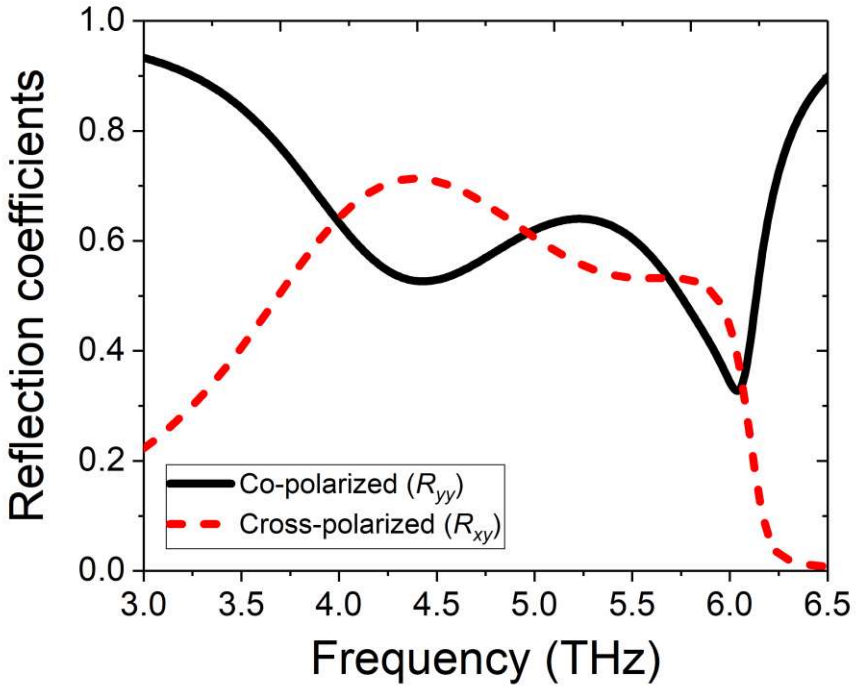

Fig. 4.3. Co-polarized (R_{yy}) and cross-polarized (R_{xy}) reflection coefficients.

because of nearly equal magnitude of the co- and cross-polarized components (R_{yy} & R_{xy}) of the wave reflected from the top graphene metasurface while the phase difference between them ($\Delta\phi$) is an odd multiple of 90° [335], [338]. The above said fact can be verified from Fig. 4.3. The axial ratio (AR) has been further computed using (4.4), where A represents the ratio of R_{yy} and R_{xy} and $\Delta\phi$ indicates the phase difference between R_{yy} and R_{xy} [335], [338]. The evaluated

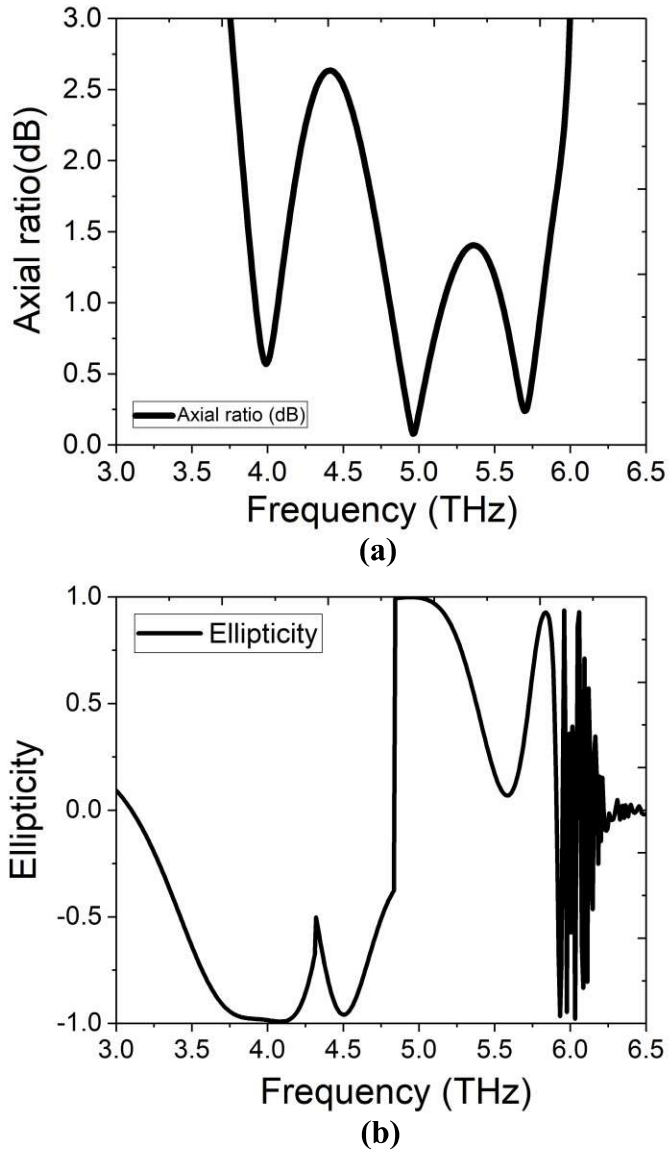

Fig. 4.4. Spectral performances in terms of (a). axial ratio (AR) and (b). ellipticity (e) of the proposed RLCPC.

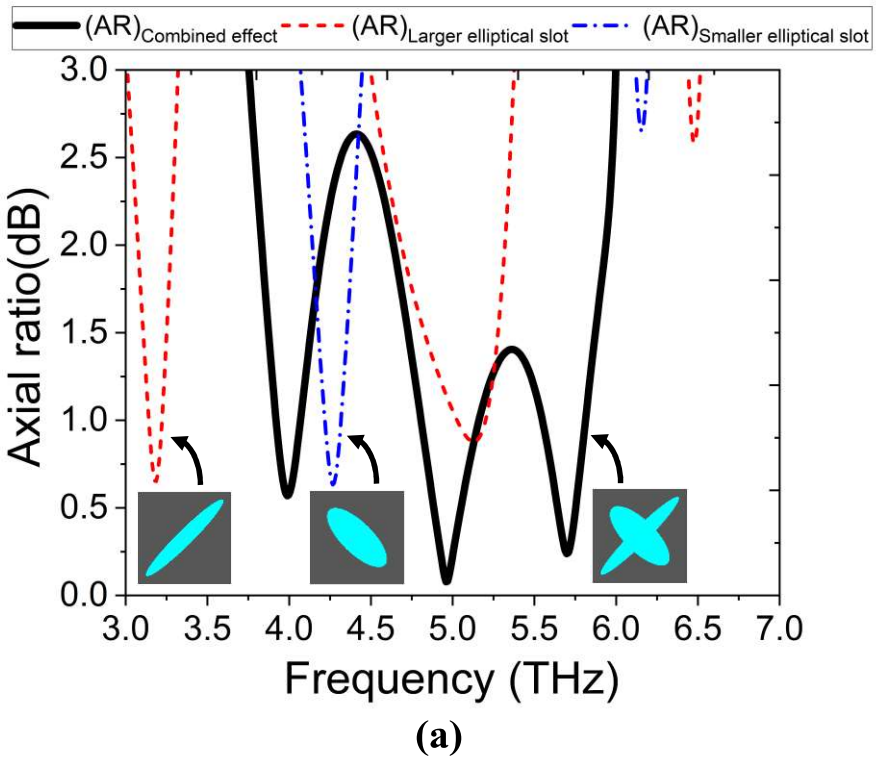

(a)

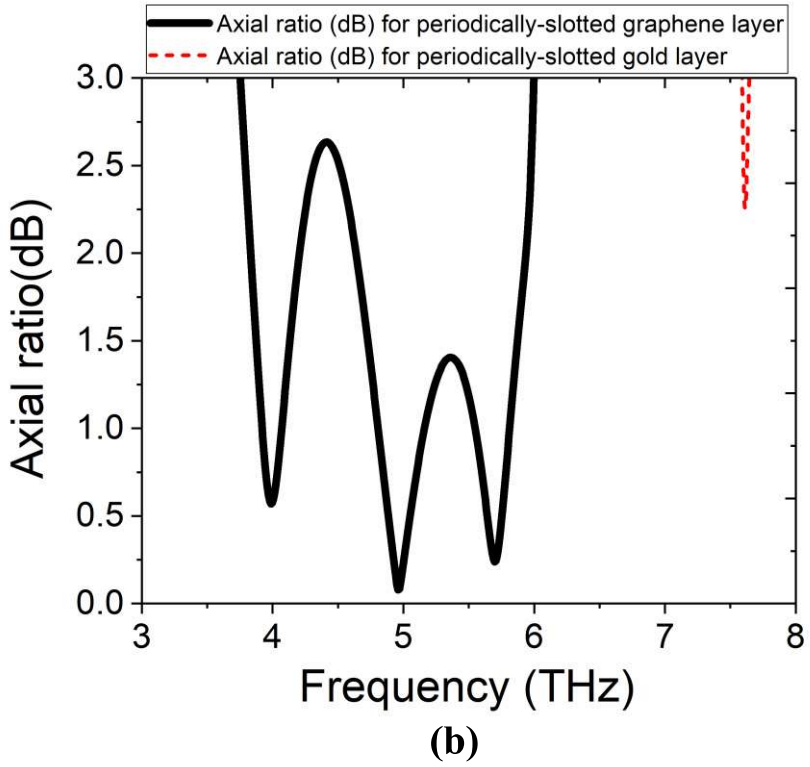

(b)

Fig. 4.5. (a). Spectral responses of axial ratio (AR) with the effect of individual elliptical slot on the unit cell of the graphene metasurface, and (b). comparison of the spectral responses of axial ratio (AR) with periodically-slotted graphene layer and periodically-slotted gold layer on top surface of the proposed RLCPC.

$$AR = \frac{\left[\frac{1}{2}\left\{R_{yy}{}^{2}+R_{xy}{}^{2}+[R_{yy}{}^{4}+R_{xy}{}^{4}+2R_{yy}{}^{2}R_{xy}{}^{2}\boldsymbol{cos}(2\Delta\boldsymbol{\varphi})]^{\frac{1}{2}}\right\}\right]^{\frac{1}{2}}}{\left[\frac{1}{2}\left\{R_{yy}{}^{2}+R_{xy}{}^{2}-[R_{yy}{}^{4}+R_{xy}{}^{4}+2R_{yy}{}^{2}R_{xy}{}^{2}\boldsymbol{cos}(2\Delta\boldsymbol{\varphi})]^{\frac{1}{2}}\right\}\right]^{\frac{1}{2}}} \qquad (4.4)$$

AR using (4.4) has been found to be less than 3-dB within 3.75 THz and 6 THz; implying that the structure behaves as a circular polarization converter (CPC) indicated in Fig. 4.4(a). The Stokes' coefficients [335] have successively been determined employing (4.5). The ellipticity (e) of the reflected EM wave has been computed from Stokes' parameters as $e = S_3/S_o$ [335]. The calculated ellipticity (e) is bounded between -1 and +1 within the desired bandwidth as seen from Fig. 4.4(b).

$$S_0 = |R_{yy}|^2 + |R_{xy}|^2$$

$$S_1 = |R_{yy}|^2 - |R_{xy}|^2$$

$$S_2 = 2|R_{yy}||R_{xy}| \cos\phi$$

$$S_3 = 2|R_{yy}||R_{xy}| \sin\phi \qquad (4.5)$$

When e = +1, the reflected wave is left-handed circularly polarized (LHCP), while e = -1 indicates a right-handed circularly polarized (RHCP) wave. It can be observed from Fig. 4.4(b) that the structure is RHCP in nature at the lower THz region while towards the higher THz spectrum, it offers LHCP. The individual elliptical slots of the meta-atom have been separately studied to provide the corresponding 3 dB AR responses as illustrated in Fig. 4.5(a). It has been observed that the periodic arrangement of the smaller elliptical slots on the top graphene surface of the proposed RLCPC exhibits two narrowband 3 dB AR minima while the larger one generates 3 dB AR minima at three distinct frequencies. The combination of both the elliptical

slots yields significantly enhanced 3 dB AR bandwidth of 2.25 THz spanning between 3.75 THz and 6 THz with 46.15% FARBW by merging the above said AR minima.

Further, the AR response with periodically-slotted graphene patterns has been compared with that of the elliptically-slotted gold pattern as provided in Fig. 4.5(b). It is evident that the use of elliptically slotted gold pattern can only generate extremely narrowband CP around 7.6 THz. Nevertheless, the use of graphene on the top surface of the metasurface design provides wideband CP conversion as evident from Fig. 4.5(b).

4.3. Validation of Simulated Responses Using Circuit Model

The structural building block of the proposed RLCPC has been examined comprising a comprehensive transmission line model owing to the unavailability of the experimental establishment. An illustration of the transmission line model for the proposed RLCPC has been presented in this section. An equivalent circuit according to the schematic has been developed for validating the electromagnetic behavior of the proposed device. The circuit component values have also been subsequently derived. The realization of the circuit model has been performed using the Keysight Advance Design System tool [298]. The schematics of the transmission line and circuit model have been illustrated in Fig. 4.6(a) and Fig. 4.6(b), respectively. The input impedance (Z_{in}) of the proposed RLCPC configuration can be derived from the basic transmission line concept [339].

$$Z = jZ_{SiO_2}\tan\left(kt_{SiO_2}\right)$$

$$Z_{in} = Z.Z_{graphene}/(Z + Z_{graphene})$$

$$Z_{in} = j(Z_{graphene}).Z_{SiO_2}\tan\left(kt_{SiO_2}\right)/(jZ_{SiO_2}\tan\left(kt_{SiO_2}\right) + Z_{graphene}) \qquad (4.6)$$

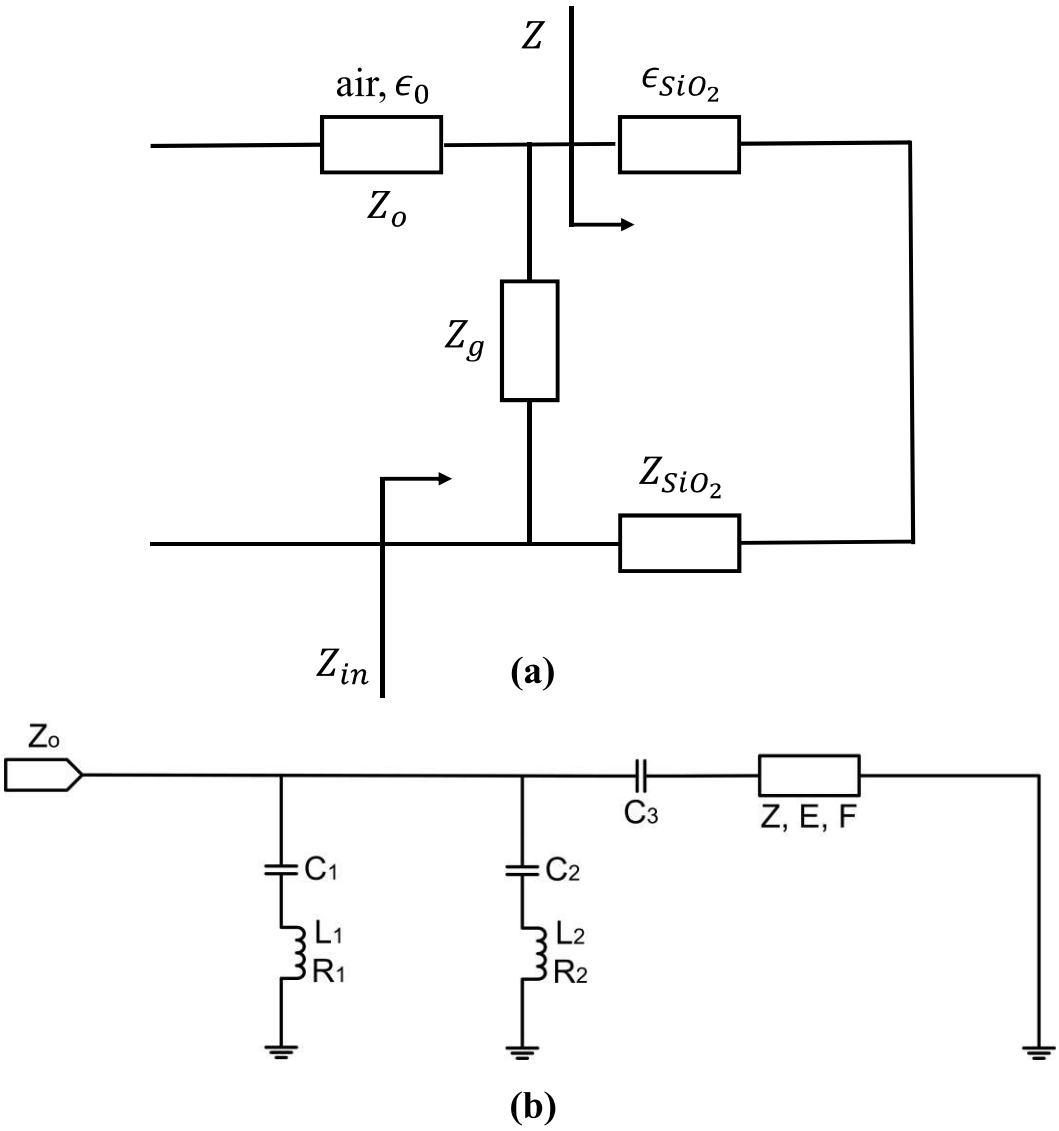

Fig. 4.6. (a). Schematic of the transmission line model for the proposed graphene-based RLCPC and (b). the circuit model representation for the transmission line schematic for the proposed RLCPC.

In (4.6), $Z_{graphene}$ represents the surface impedance of the top graphene metasurface, the input impedance for the SiO_2 substrate is Z. Z_{in} points to the input impedance of the proposed device, while the characteristics impedance of the SiO_2 substrate is interpreted as Z_{SiO_2}, The thickness of the SiO_2 substrate bearing the graphene metasurface is termed as t_{SiO_2} ($t_{SiO_2} = t = 12$ µm), ϵ_{SiO_2} is denoting the relative permittivity of the SiO_2 substrate and k is the propagation constant

of the electromagnetic wave within the said substrate. The co-polarized reflection coefficient (Γ_{co}) for the proposed device can be derived using equation (4.7).

$$|\Gamma_{co}| = R_{yy} = \left|\frac{Z_{in}-Z_o}{Z_{in}+Z_o}\right| \qquad (4.7)$$

The input of the circuit network has been connected to the free space impedance (Z_o) as the EM wave is incident from the free space. The top graphene metasurface with the periodic

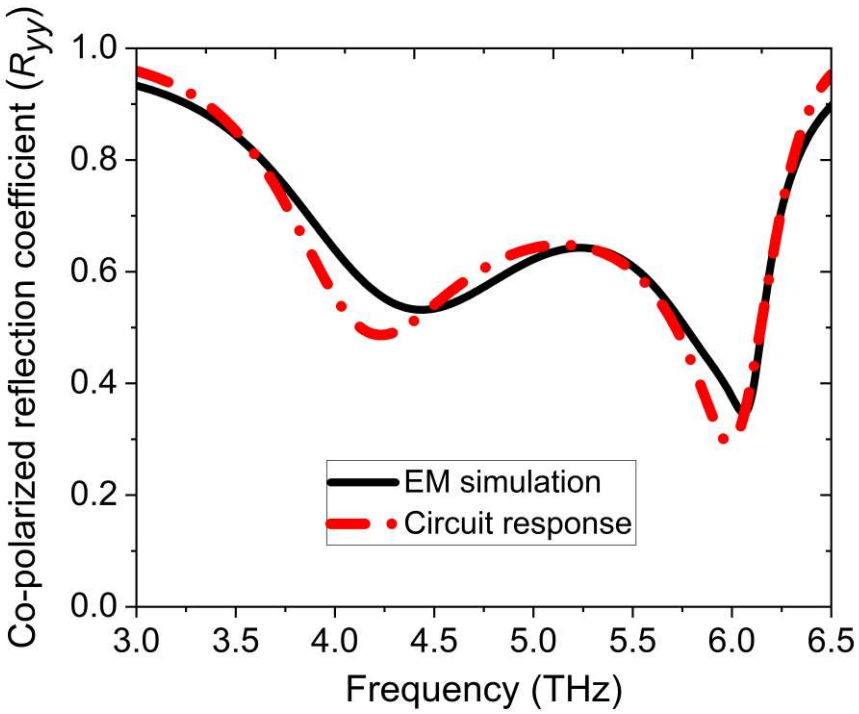

Fig. 4.7. Similar co-polarized reflection coefficients (R_{yy}) extracted from the circuit model of the RLCPC, as compared to the EM simulated results.

elliptical slots can be considered as a combination of two distributed R-L-C circuit components (R_1, L_1, C_1 and R_2, L_2, C_2) [293], connected in parallel with the original circuit, as described in Fig. 4.6(b). The resistive components (R_1 and R_2) have been introduced to take care of the losses owing to the periodically slotted graphene metasurface. The circuit model also includes the coupling capacitance (C_3) between the top graphene metasurface and the bottom gold layer. The parasitic capacitance between the unit cells has been neglected in this case as the span of

the graphene metasurface is continuous on the SiO_2 substrate. The SiO_2 substrate has been represented by a transmission line stub as a function of the parameters, Z, E and F, where Z = Z_{SiO_2}, E = phase of the EM wave and F stands for one of the frequency instances within the spectral range of operation. It now incorporates the realistic substrate, i.e., silicon dioxide (SiO_2) as it accounts for the accurate phase change (E) of the transmission line used in the circuit model. The loss in the silicon dioxide (SiO_2) substrate has been taken care of by the impedance term Z. The other end of the transmission line stub has been connected to the ground as the bottom gold surface of the structural configuration of the proposed device hinders the transmission of the EM wave. The values of the circuit components have been included in Table 4.2. One can determine a good resemblance between the electromagnetic simulated (EM) output and the response evaluated from the circuit model in Fig. 4.7.

The electric field distribution of the proposed meta-atom has been studied at 3.98 THz, 4.98 THz, and 5.68 THz as shown in Figs. 4.8(a)-(c). It can be observed that electric fields are confined (magneto-plasmonic field distribution) at the slotted region owing to the formation of field localization during the wave- matter interaction process [340]-[342] at the interface between graphene metasurface and SiO_2 substrate. In accordance with the field distribution

Table 4.2. Optimized Values for the Circuit Components

Proposed RLCPC (R-L-C Components)	Optimized Values for the R-L-C Components
C_1	284.197 fF
C_2	0.0535 fF
C_3	336.1038 fF
L_1	10.399 pH
L_2	16.096 pH
R_1	1 Ω
R_2	91.9 Ω
Z	248.586 Ω
E	123.5°
F	4.75 THz

patterns, graphene surface plasmons (GSPs) are excited mostly over the perimeter of the smaller slots owing to the electric field concentration at 3.98 THz. GSPs are excited to a great

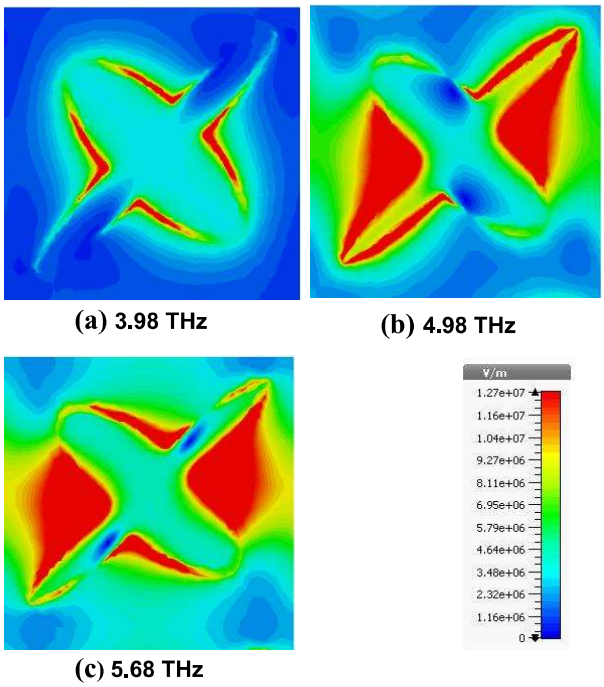

Fig. 4.8. (a)-(c). Wave-matter interaction on the slotted graphene layer placed on top of SiO_2 substrate of the proposed RLCPC (Magneto-plasmonic case) at 3.98 THz, 4.98 THz and 5.68 THz, respectively.

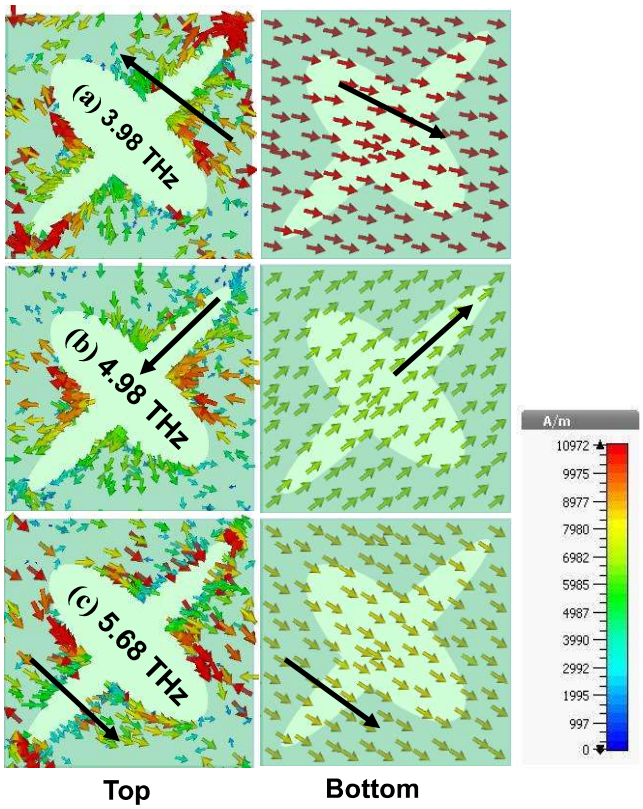

Fig. 4.9. (a)-(c). Surface current distributions of the proposed RLCPC at 3.98 THz, 4.98 THz and 5.68 THz, respectively.

extent but diagonally distributed over the combined slots at 4.98 THz. In case of 5.68 THz, GSPs are excited highly over both the elliptical slots because of the confinement of the electric fields. Further, the surface currents at the top and bottom layers of the meta-atom design have been studied and illustrated in Figs. 4.9(a)-(c). It has been revealed from Fig. 4.9 that at 3.98 THz and 4.98 THz, the surface currents are anti-parallel in nature at the two layers; thereby forming magnetic resonance.

4.4. Ultrawideband Tunability Delivered by the RLCPC

The proposed device offers tunable characteristics in the spectral domain by altering the chemical potential (μ) of the graphene metasurface. The chemical potential (μ) can be varied by applying different external stimuli [97]-[99]. A simple but effective biasing scheme has

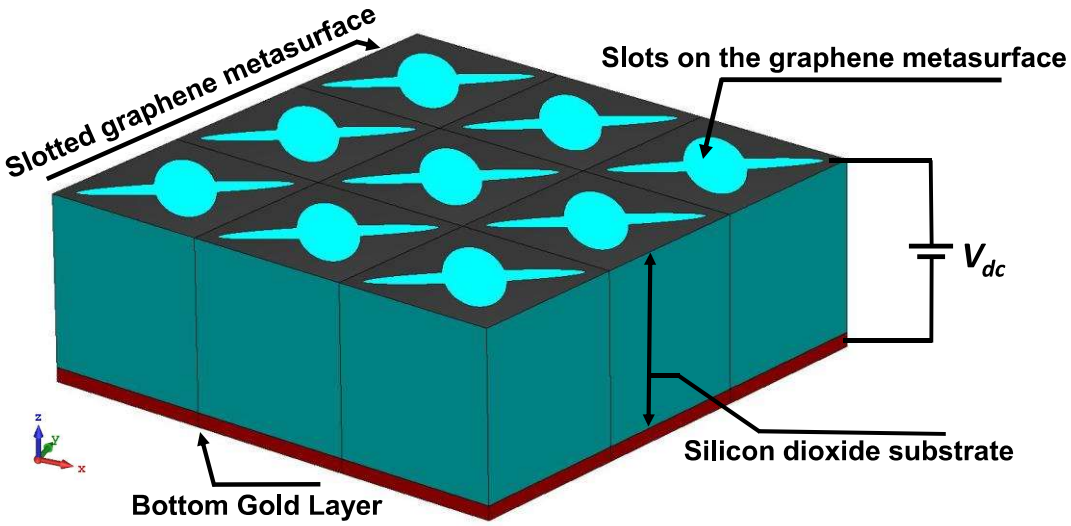

Fig. 4.10. A probable biasing scheme for the proposed RLCPC.

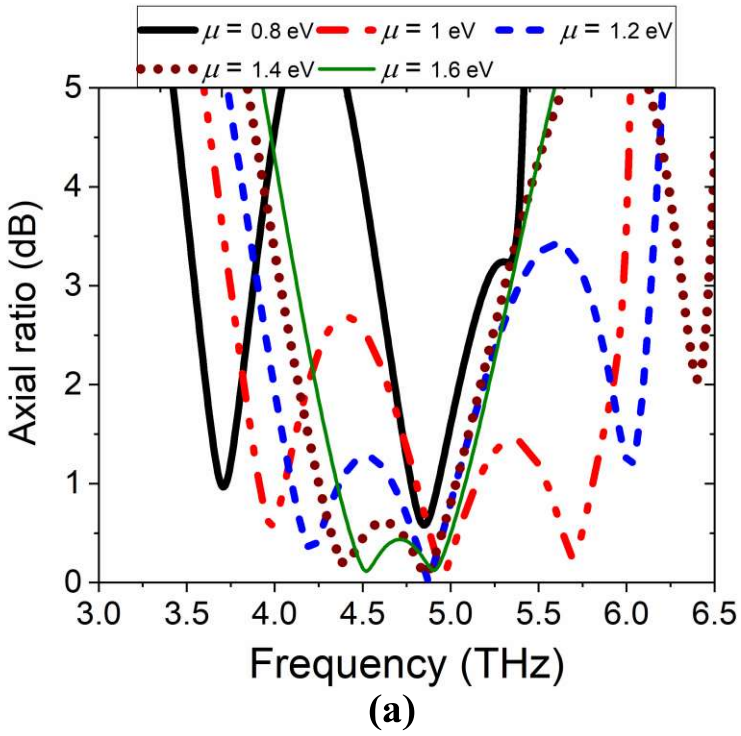

(a)

Fig. 4.11. Variation of AR of the EM wave reflected from the proposed RLCPC under different chemical potential values (μ).

been presented in Fig. 4.10, where the periodically slotted continuous graphene metasurface is connected to the bottom gold surface via a dc biasing voltage, V_{DC}. The values of V_{DC} can be changed by applying an external static electric field [26]. A change in μ results in the shift of

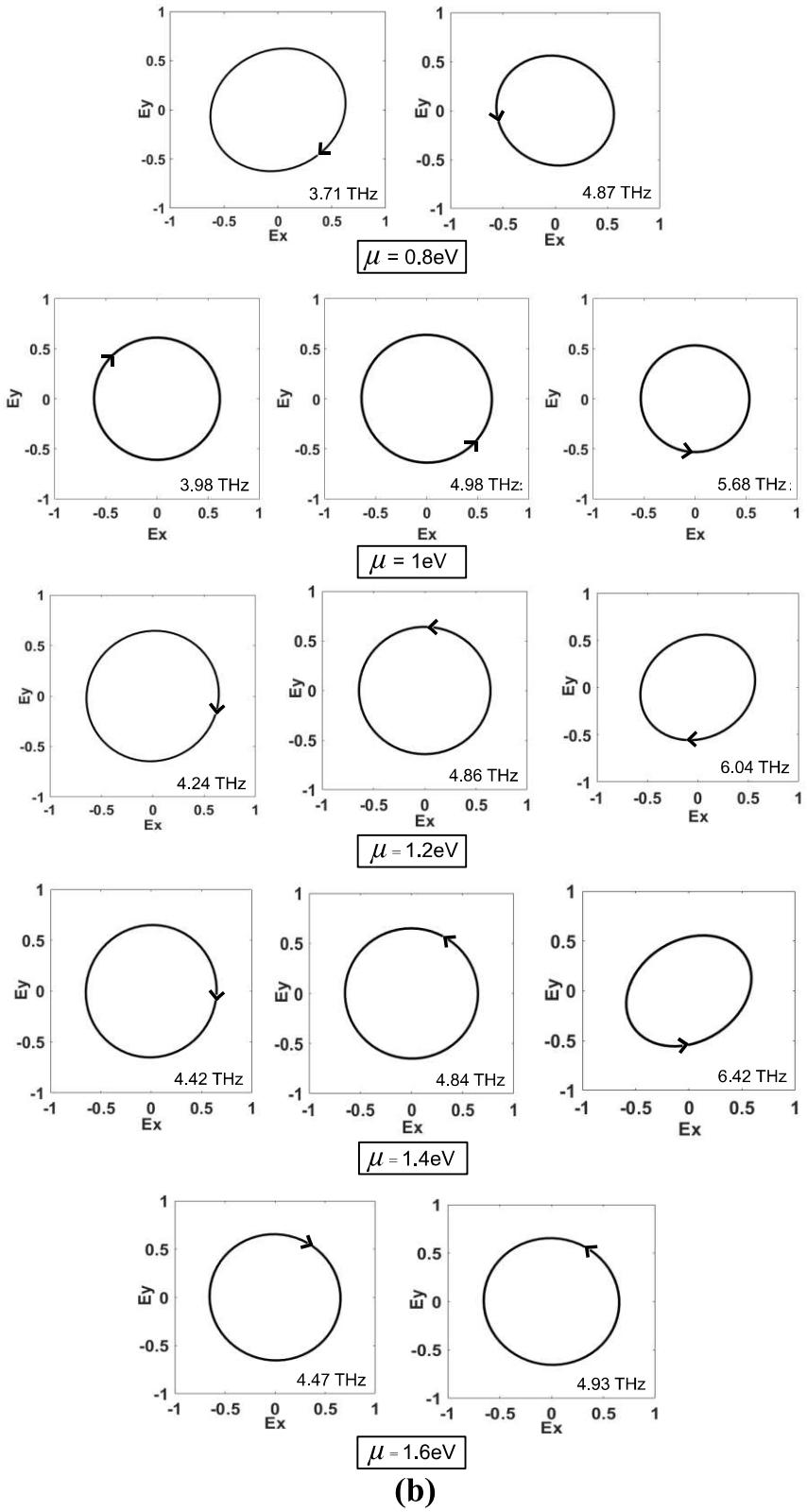

(b)

Fig. 4.12. Variation of AR of the EM wave reflected from the proposed RLCPC under different polarization ellipses formed at different frequencies at the reflection end of the proposed RLCPC while varying the chemical potential (μ) induced by the variable biasing voltage V_{dc}.

graphene's Fermi level [26], [159], which further changes the spatial mobility and electrical conductivity in graphene metasurface. This leads to the change in magnitudes of the co- and cross-polarized reflection coefficients (R_{yy} and R_{xy}). Therefore, the corresponding AR responses are getting changed to provide a tunable property, as shown in Fig. 4.11. The Fermi level of graphene can be changed by applying an external variable biasing voltage between the top periodic graphene pattern and bottom gold layer [155]. During the optimization process, a range of chemical potential (μ) values have been chosen to study the different AR responses within the desired spectral region. The optimized FARBW has been achieved at μ = 1eV, which is an advantage of the proposed RLCPC; as beyond μ = 1eV has not been realized in practice till date [343]. Further, the polarization ellipses have been generated using an inhouse code for experiencing the orientation of the reflected wave from the proposed RLCPC at different

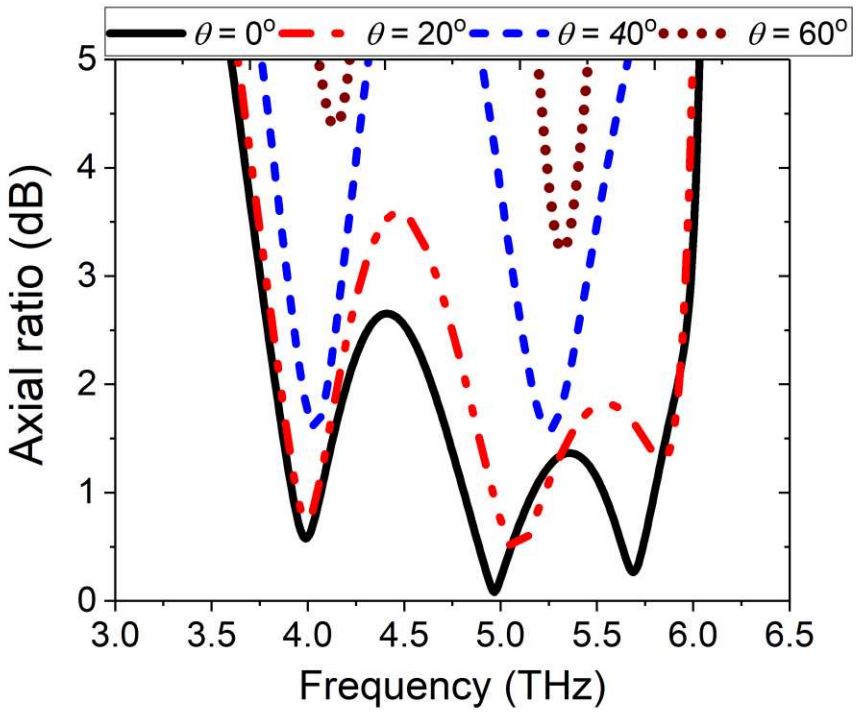

Fig. 4.13. Variation of AR of the EM wave reflected from the proposed RLCPC under different oblique incidences (θ) of EM wave.

frequencies for different chemical potential values as described in Fig. 4.12. It can be concluded that the shape of most of the polarization ellipses are circular in nature as the axial ratios are extremely close to 0 dB at different frequencies as observed from Fig. 4.12. A few polarization ellipses are in elliptical shape owing to the AR dips are away from 0 dB at 3.71 THz, 6.04 THz and 6.42 THz for μ = 0.8eV, μ = 1.2eV and μ = 1.4eV respectively, as illustrated in Fig. 4.12. The polarization ellipse at 3.98 THz is RHCP as the ellipticity (e) is equal to -1, as confirmed from Fig. 4.12. In some of the cases, the polarization ellipses are LHCP in nature as the ellipticity (e) is equal to +1, also confirmed from Fig. 4.12, etc. The angular stability of the proposed RLCPC was examined as provided in Fig. 4.13. It has been observed that satisfactory performance of the structure can be realized till 40° incident angle of the EM wave.

Transmittive-type triple-band linear to circular polarization conversion in THz region using graphene-based metasurface

In this section, a graphene-based transmittive-type triple band linear to circular polarization converter (TTLCPC) has also been proposed in the lower mid-infrared (MIR) region covering the terahertz gap. In this proposed design, the periodic graphene patches on top of the silicon dioxide (SiO_2) substrate manipulate the incident EM wave to enter into the proposed device with its maximum efficiency. Maximum possible entry of the wave takes place due to the impedance matching between the top graphene surface and free space. As per performance, it is better than any other metallic counterparts in this case. At the opposite side of the substrate, an array of specifically-shaped slots is generated from the bottom gold layer to have moderate transmission of EM wave with three axial ratio (AR) minima at three different frequencies *viz.*, 5.72 THz, 13.49 THz and 18.90 THz in the lower terahertz domain. The specific patterning of the device provides generation of circularly polarized (CP) wave while the incident wave is of linearly polarized (LP) in nature as the AR computed from the response has been found to be less than 3 dB. The proposed design offers angular stability till 40° incident angle. The proposed TTLCPC can be used for various applications in terahertz domain including spectroscopy, defense and imaging applications [344]-[347].

4.5 Theory of Transmittive Polarization of EM Wave

The linearly polarized electric field of the incident wave propagating along z-direction with angular frequency ω, wave vector k and complex amplitudes I_x, I_y can be expressed as given in equation (4.8).

$$E_i(r,t) = \begin{bmatrix} I_x \\ I_y \end{bmatrix} e^{i(kz-\omega t)} \qquad (4.8)$$

The Jones Matrix $J = \begin{bmatrix} I_x \\ I_y \end{bmatrix}$ signifying the polarization state of the incident wave can be expressed by equation (2) when the incident electric field is LP in nature making an angle θ with respect to x-axis. Jones matrices corresponding to right-handed circularly polarized (RHCP) and left-handed circularly polarized (LHCP) are given in equations (3) and (4) respectively [348]

$$J = \begin{bmatrix} Cos\ \theta \\ Sin\ \theta \end{bmatrix}_{LP} \qquad (4.9)$$

$$J = 1/\sqrt{2} \begin{bmatrix} 1 \\ -i \end{bmatrix}_{RHCP} \qquad (4.10)$$

$$J = 1/\sqrt{2} \begin{bmatrix} 1 \\ i \end{bmatrix}_{LHCP} \qquad (4.11)$$

The transmitted electric field can be formulated as given in equation (4.12) where f denotes the propagation of the wave in the positive z-direction and lin implies special linear base where all the base vectors are parallel to the coordinate axes.

$$E_t(r,t) = \begin{bmatrix} T_x \\ T_y \end{bmatrix} e^{i(kz-\omega t)} \quad (4.12)$$

$$\begin{bmatrix} T_x \\ T_y \end{bmatrix} = \begin{bmatrix} T_{xx} & T_{xy} \\ T_{yx} & T_{yy} \end{bmatrix} \begin{bmatrix} I_x \\ I_y \end{bmatrix} = T_{lin}^{f} \begin{bmatrix} I_x \\ I_y \end{bmatrix}$$

For a medium with no linear polarization effect, the conditions in equation (5) will become $T_{xy} = 0$ and $T_{yx} = 0$ to give rise to equation (4.13).

$$\begin{bmatrix} T_x \\ T_y \end{bmatrix} = \begin{bmatrix} T_{xx} & 0 \\ 0 & T_{yy} \end{bmatrix} \begin{bmatrix} I_x \\ I_y \end{bmatrix}$$

$$\begin{bmatrix} T_x \\ T_y \end{bmatrix} = \begin{bmatrix} T_{xx} I_x \\ T_{yy} I_y \end{bmatrix} \qquad (4.13)$$

For efficient conversion of incident LP wave into the CP one, the magnitudes of T_x and T_y should be equal along with an odd-integral multiple of 90° phase difference between them. Considering Jones matrix of an incident wave exhibiting LP, equation (4.14) has been derived.

$$\frac{|T_{xx}|}{Sin\,\theta} = \frac{|T_{yy}|}{Cos\theta} \qquad (4.14)$$

From the knowledge of the transmitted electric field components, the Stokes' parameters are evaluated as shown in equation (4.15), where T_x and T_y are the co- and cross-polarized transmitted electric field components and φ is the angle between them [335], [349].

$$S_0 = |T_y|^2 + |T_x|^2$$

$$S_1 = |T_y|^2 - |T_x|^2$$

$$S_2 = 2|T_x||T_y|\,cos\,\varphi$$

$$S_3 = 2|T_x||T_y|\,sin\,\varphi \qquad (4.15)$$

4.6 Design of the Device

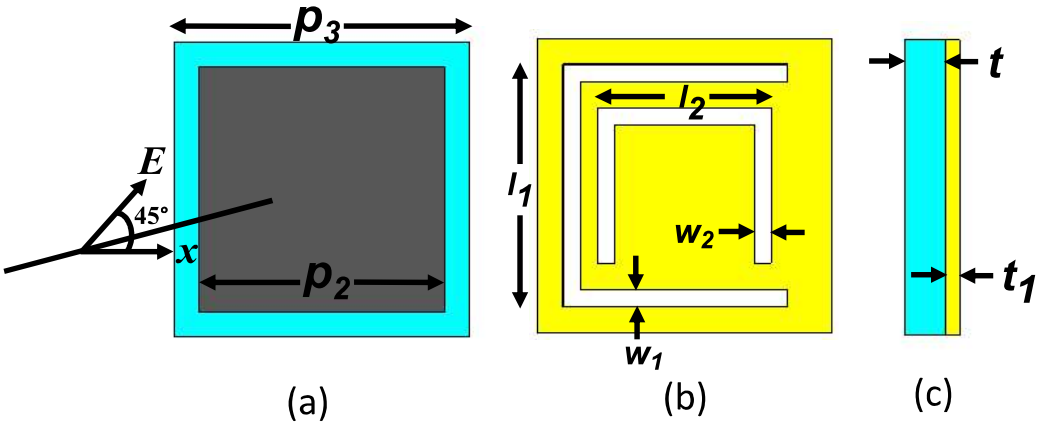

Fig. 4.14. (a) Top view, (b) bottom view and (c) side views of the unit cell of the proposed graphene-based TTLCPC in terahertz gap (l_1 = 14 µm, l_2 = 7 µm, w_1 = 1.3 µm, w_2 = 1.3 µm, p_2 = 10 µm, p_3 = 12 µm, t = 2 µm, t_1 = 0.5 µm).

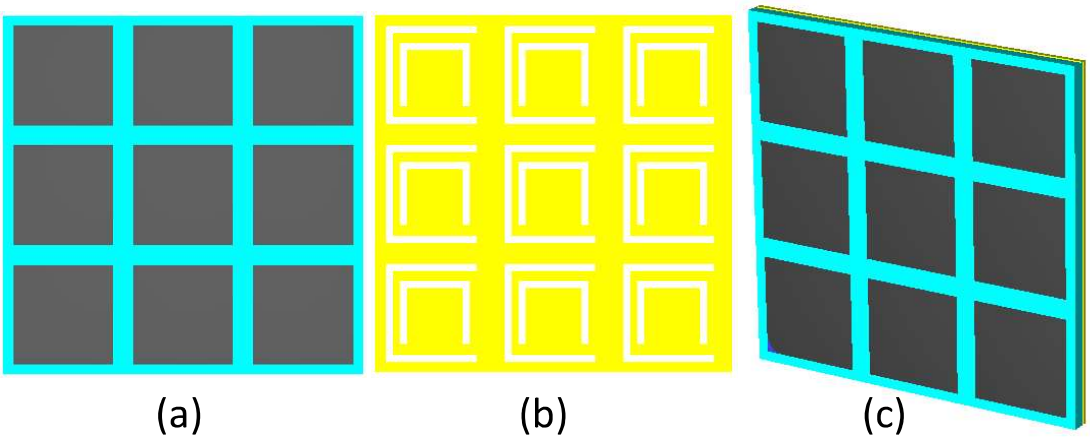

Fig. 4.15. (a) Top view, (b) bottom view and (c) perspective view of the proposed realizable graphene-based TTLCPC.

Table 4.3. Materials/Metals Used in the Formation of the Device

Materials/Metal	Properties
Graphene metasurface	(t_g = 1 nm, T = 300 K, μ_c = 1 eV, τ = 1 ps, p_2 = 10 µm)
Silicon dioxide substrate (SiO_2)	(ε_r = 3.9, tan δ= 0.0006, t = 2 µm)
Slotted Background (Metallic gold)	($\sigma_{elect.}$ = 4.56×10^7 S/m, t_1 = 0.5 µm)
Metallic square-shaped gold patches	($\sigma_{elect.}$ = 4.56×10^7 S/m, t_1 = 0.5 µm)

The unit cell of the proposed design comprises 1 nm thick square-shaped graphene layer deposited on a 2 µm thick silicon dioxide (SiO_2) substrate (relative permittivity of 3.9 and $tan\,\partial = 0.0006$) while the backside of the SiO_2 is covered with a specifically-slotted gold layer. The top, bottom and side views of the proposed transmittive-type nanodevice are shown in Fig. 4.14(a), Fig. 4.14(b) and Fig. 4.14(c) respectively. The whole device is a periodic arrangement of the above-said unit cell and the illustration of the proposed realizable device is shown in Fig. 4.15. The electromagnetic wave is incident normally to the graphene patch as

shown in Fig. 4.14 where the electric field is polarized at an angle of 45° with respect to the *x*-axis. The details regarding the properties of the materials used in this manuscript have been provided in in Table 4.3 where t_g is thickness of graphene layer and rest all the parameters are described in this manuscript.

The proposed device can be represented using an equivalent impedance circuit model. The periodically distributed graphene patches deposited on the SiO_2 substrate as depicted in Fig. 4.16. The impedance of the periodic graphene patch is approximated as presented in equation (4.16). r_g and l_g are resistance and inductance of the single graphene patch and they can be modulated by making the variation in chemical potential (μ) of the graphene surface. c_g is derived from the mutual coupling between the adjacent square graphene patches [292].

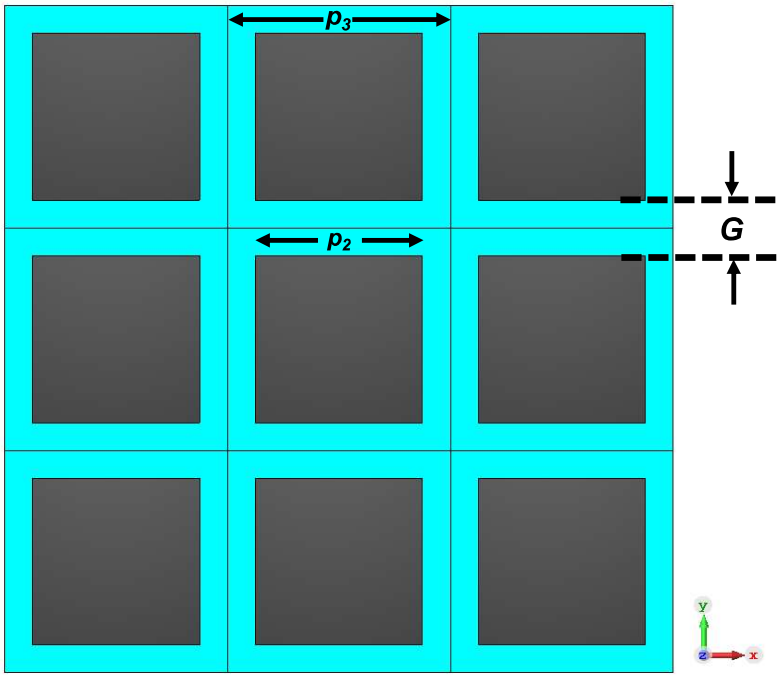

Fig. 4.16. Geometry of the top surfaced square graphene patches

$$Z_{patch}(\omega) = r_{graphene} + j\omega l_{graphene} + \frac{1}{j\omega c} \qquad (4.16)$$

$$r_g = \frac{a[p_3]^2}{(p_3 - G)^2} . Re[\sigma_g]^{-1} \qquad (4.17)$$

$$l_g = \frac{a[p_3]^2}{(p_3-G)^2} \cdot \frac{Im[\sigma_g]^{-1}}{\omega} \qquad (4.18)$$

$$c_g = \frac{2p_3\varepsilon_{eff}}{\pi} \cdot \ln\left[\csc\left\{\frac{\pi G}{2p_3}\right\}\right] \qquad (4.19)$$

Here, p_3 = periodicity of the unit cell, G = separation between the square graphene patches, σ_g = Drude conductivity of graphene, a is the weighted coefficient, $\varepsilon_{eff} = \frac{\varepsilon_0(1+\varepsilon_h)}{2}$ = permittivity of the media surrounding the periodic square-shaped graphene patches, ε_0 = permittivity of the free space and ε_h = relative permittivity of the SiO_2 substrate [350]. The top graphene surface shown in Fig. 4.16 is represented by an equivalent impedance Z_g which is a series combination of resistance, inductance and capacitance, *viz*., r_g, l_g and c_g respectively, as described in Fig. 4.17. The SiO_2 substrate can be represented by a dielectric spacer of permittivity ε_h and impedance of Z_h . The specifically slotted backside metallic gold plate can be represented by a bandpass filter which is a parallel circuit combination of inductance l_b and capacitance c_b.

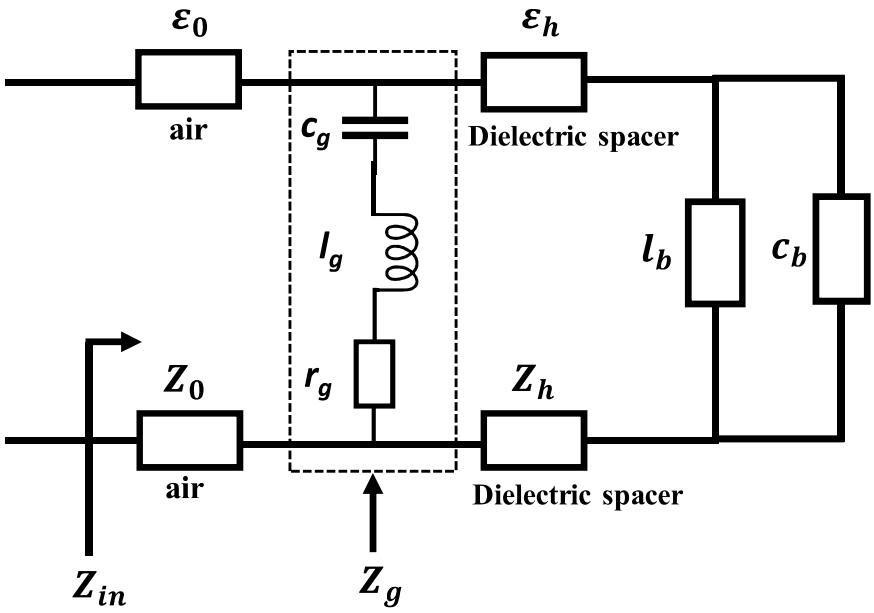

Fig. 4.17. Equivalent circuit model of the unit cell of the proposed TTLCPC

4.7 Simulated Results

The unit cell given in Fig. 4.14 has been simulated employing periodic boundary conditions in CST Microwave Studio using a mesh with 38,506 tetrahedra. The frequency responses of the amplitude of resultant co-polarized (T_x) and cross-polarized (T_y) transmitted electric field components are shown in Fig. 4.18(a). It is seen from Fig. 4.18(a) that T_x and T_y possess equal magnitude at 5.72 THz, 13.49 THz, and 18.90 THz. The phase-difference between T_x and T_y are -90°, +90° and -90° respectively at the aforementioned frequencies as depicted from the phase spectra in Fig. 4.18(b). The axial ratio (AR) can further be computed from equation (4.20) where T_x and T_y are the magnitude of the transmitted co- and cross-polarized components and $\Delta\phi$ = phase difference between them; as illustrated in Fig. 6 which clearly indicates that AR is below 3 dB at these three distinct frequencies signifying that the transmitted wave is CP in nature [243]. In Fig. 4.18(a), the magnitude of the transmitted co- and cross-polarized components of the transmission coefficients (T_x and T_y) have been represented. They intersect at three distinct frequencies, viz., 5.72 THz, 13.49 THz, and 18.90 THz, respectively. On the other hand, the phases of the co- and cross-polarized transmitted coefficients of the wave are provided in Fig. 4.18(b). The phase difference ($\Delta\phi$) between them has also been illustrated in Fig. 4.18(b). It can be observed that the phase-difference at the frequencies mentioned above is 90˚.

$$AR = \frac{\left[\frac{1}{2}\left\{T_y{}^2+T_x{}^2+[T_y{}^4+T_x{}^4+2T_y{}^2T_x{}^2\boldsymbol{cos}(2\Delta\boldsymbol{\varphi})]^{\frac{1}{2}}\right\}\right]^{\frac{1}{2}}}{\left[\frac{1}{2}\left\{T_y{}^2+T_x{}^2-[T_y{}^4+T_x{}^4+2T_y{}^2T_x{}^2\boldsymbol{cos}(2\Delta\boldsymbol{\varphi})]^{\frac{1}{2}}\right\}\right]^{\frac{1}{2}}} \qquad (4.20)$$

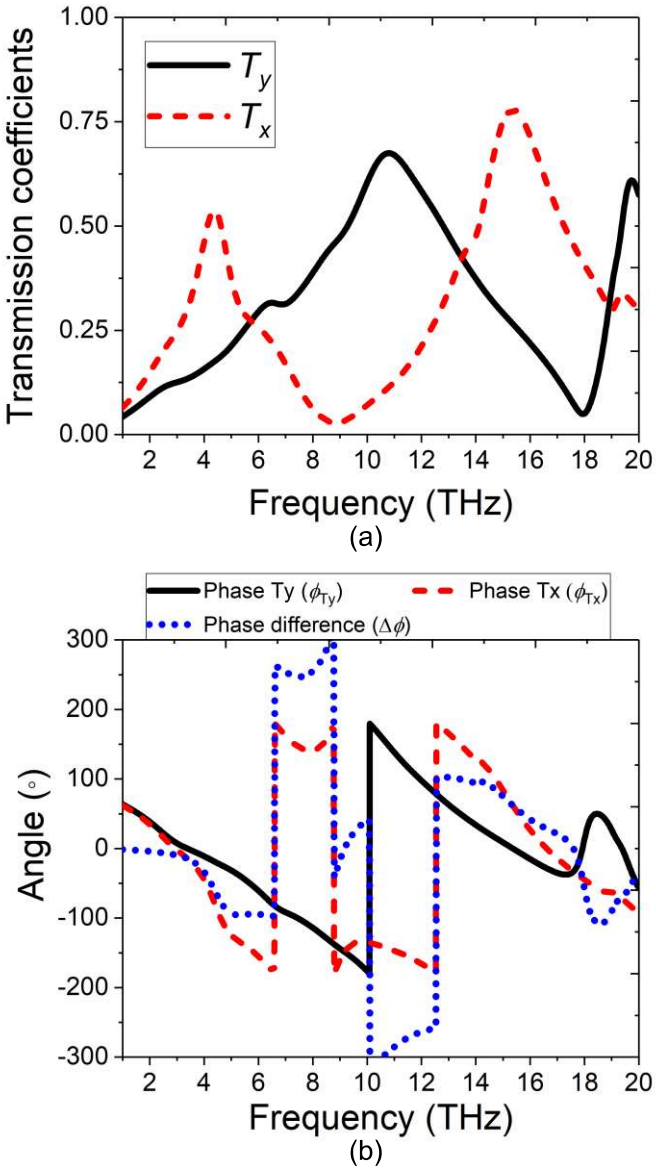

Fig. 4.18. Frequency responses of the proposed TTLCPC in terms of (a) transmission coefficients (T_x & T_y) and (b) phase difference between them (T_x & T_y).

The ellipticity (e) can be subsequently computed from equation (4.15) as $e = S_3/S_0$. The frequency response of e has been given in Fig. 4.20. It is seen that at 5.72 THz, 13.49 THz, and 18.90 THz, the respective e values are close to +1, -1 and +1 shown as depicted from Fig. 4.20;

which imply that the CP behaves as LHCP at 5.72 THz and 18.90 THz while RHCP nature has been observed at 13.49 THz. If the periodic gold patches are deposited at the top surface instead of the graphene layer, the CP nature could not be achieved. It can be seen from Fig. 4.21 that

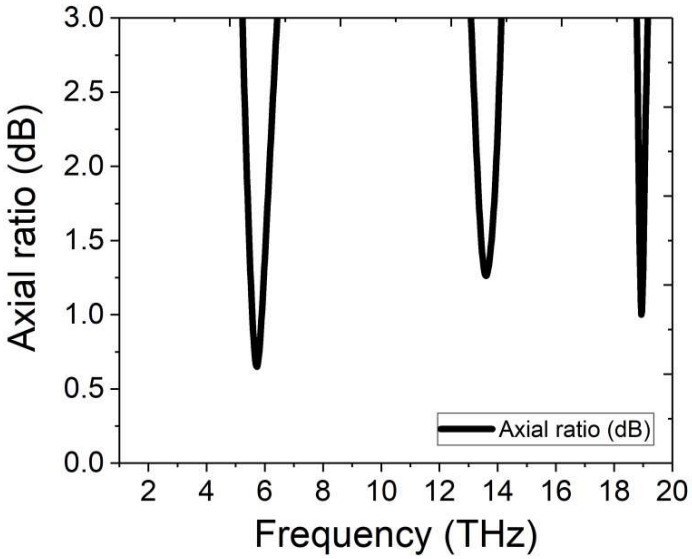

Fig. 4.19. Frequency response of the proposed TTLCPC in terms of Axial ratio (AR) under 3 dB at 5.72 THz, 13.49 THz and 18.90 THz respectively.

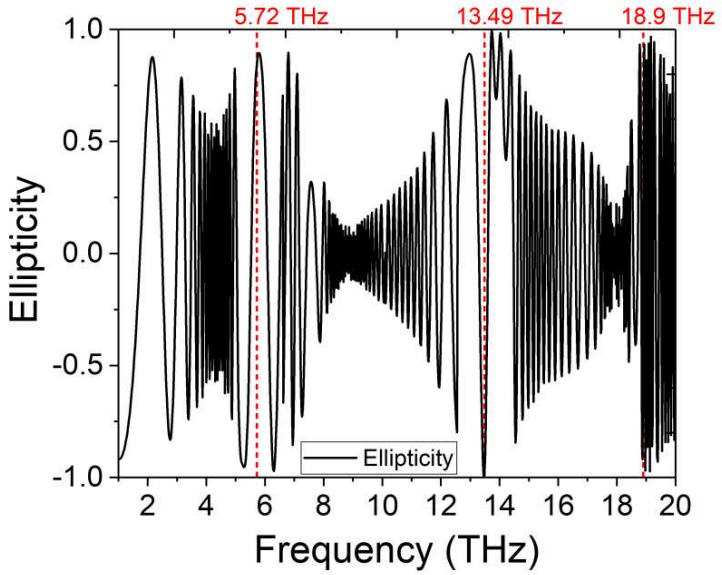

Fig. 4.20. Frequency response of the proposed TTLCPC in terms of ellipticity (*e*) within the whole frequency band.

the AR does not fall below 3 dB within the terahertz gap while the graphene counterpart provides multiple dips of AR below 3 dB indicating generation of CP at the three distinct frequencies. The AR responses of the proposed TTLCPC device comprising graphene metallic

pattern at the top layer have been compared with those of the metal counterparts as shown in Fig. 4.21. The periodic graphene patches provide triple-band linear to circular polarization conversion of the EM wave in between 1 THz and 20 THz providing the AR dips under 3 dB at 5.72 THz, 13.49 THz, and 18.90 THz, respectively, as shown in solid black line in Fig. 4.21. Now, if the graphene patches are replaced with identical gold patches, the AR curve is far above 3 dB only

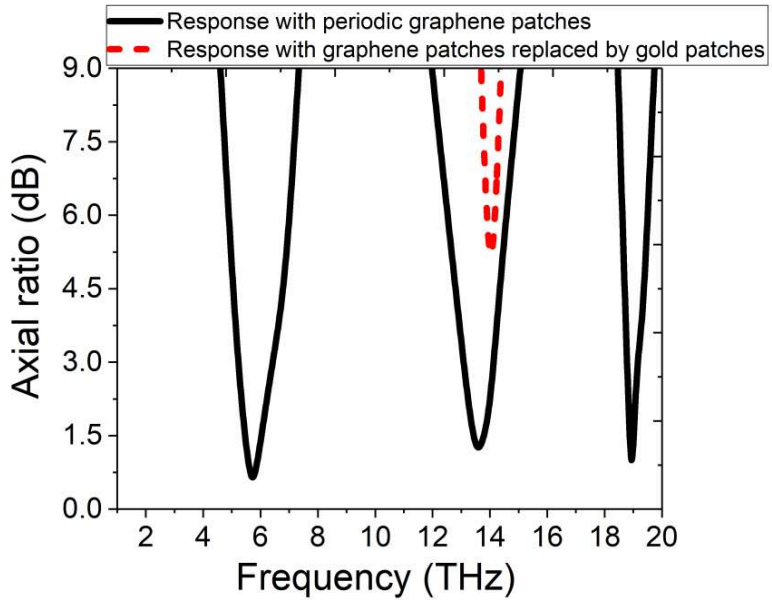

Fig. 4.21. Frequency response of the proposed TTLCPC in terms of Axial ratio (AR) with periodic graphene patches and when graphene patches are replaced by gold patches.

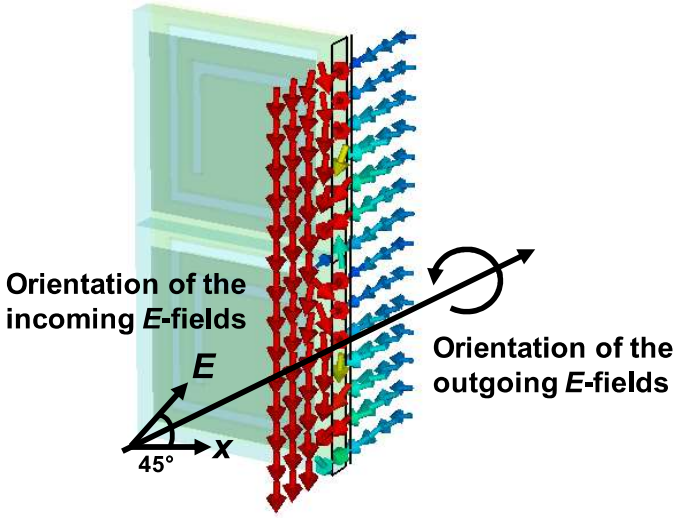

Fig. 4.22. The orientation of the incident and transmitted *E*-fields through the proposed TTLCPC.

at a single frequency close to 14 THz, which implies that the transmitted EM wave is not circularly polarized at any of the specific bands mentioned previously, as shown in red dashed line in Fig. 4.21. May be, this is experienced due to the stronger coupling between the top periodic graphene metasurface and specifically-slotted bottom gold layer than the coupling between the differently patterned top and bottom gold layers in the second case illustrated in Fig. 4.21. The incident electric field vector (*E*-field) of the incoming wave is linearly polarized while the outgoing *E*-field is circularly polarized. At a particular phase, the phenomena can be represented in Fig. 4.22.

4.9.1 Discussions

To understand the mechanism of the conversion of LP to CP, the electric field distribution has been studied on the top surface of the proposed device as shown in Fig. 4.23. Surface plasmonic resonance has been observed in the graphene patch where different parts of the graphene surface associated with the SiO_2 substrate take part in the electromagnetic wave-structure interaction process. It can be observed from Fig. 4.23 that the electric fields are highly concentrated on the top graphene patch at 5.72 THz, 13.49 THz and 18.90 THz. The individual smaller U-shaped slot provides the AR dip under 3 dB at the highest transmitting band at around 18 THz. The larger U-shaped slot provides AR dip under 3 dB at the highest and the second-highest transmitting band at around 18 THz and 13 THz, respectively. The combination of the two U-shaped slots provides three transmitting bands having an axial ratio (AR) under 3dB. The third transmitting band at 5.72 THz is generated due to the coupling between the two differently shaped U-shaped slots on the bottom gold surface.

The above-said fact can be verified from the field distribution diagram in Fig. 4.23. The field concentration is high around the smaller slot on the ground plane at 18.90 THz. The field concentration is high around the larger slot on the ground plane at 13.49 THz. At 5.72 THz,

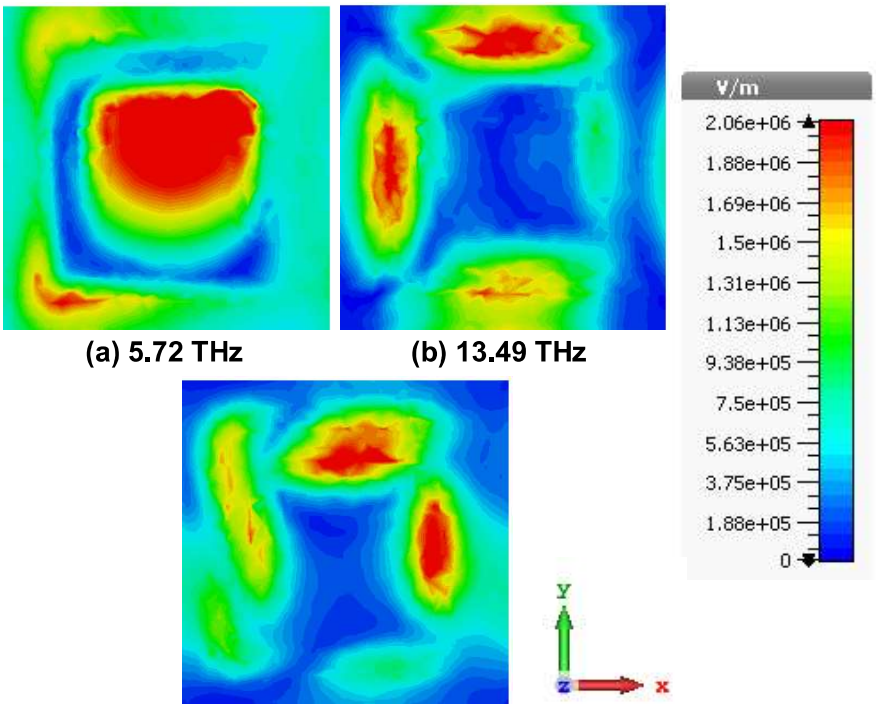

Fig. 4.23. Wave-structure interaction on the graphene layer placed on top of the SiO_2 substrate of the proposed TTLCPC at different plasmonic resonant frequencies.

the field concentration is high around the smaller and larger slots on the ground plane. This fact validates that this transmitting mode at 5.72 THz has been generated due to the coupling between the other two modes. Polarization ellipses have been formed at the transmitting end of the proposed TTLCPC at 5.72 THz, 13.49 THz and 18.90 THz as demonstrated in Fig. 4.24. It has been revealed that the polarization ellipses are very close to circular in nature at 5.72 THz and 18.90 THz as the axial ratio is very close to 0 dB. Due to finite AR in logarithmic scale at 13.49 THz, the polarization ellipse gets slightly deviated from the circular nature.

The proposed structure has been studied under various geometrical parameters. First, the frequency responses of AR have been studied under different dimensions of the top graphene patch (p_2), as illustrated in Fig. 4.25(a) while the other structural parameters remain constant. The alterations in p_2 result in slight change in the coupling strength between the top graphene

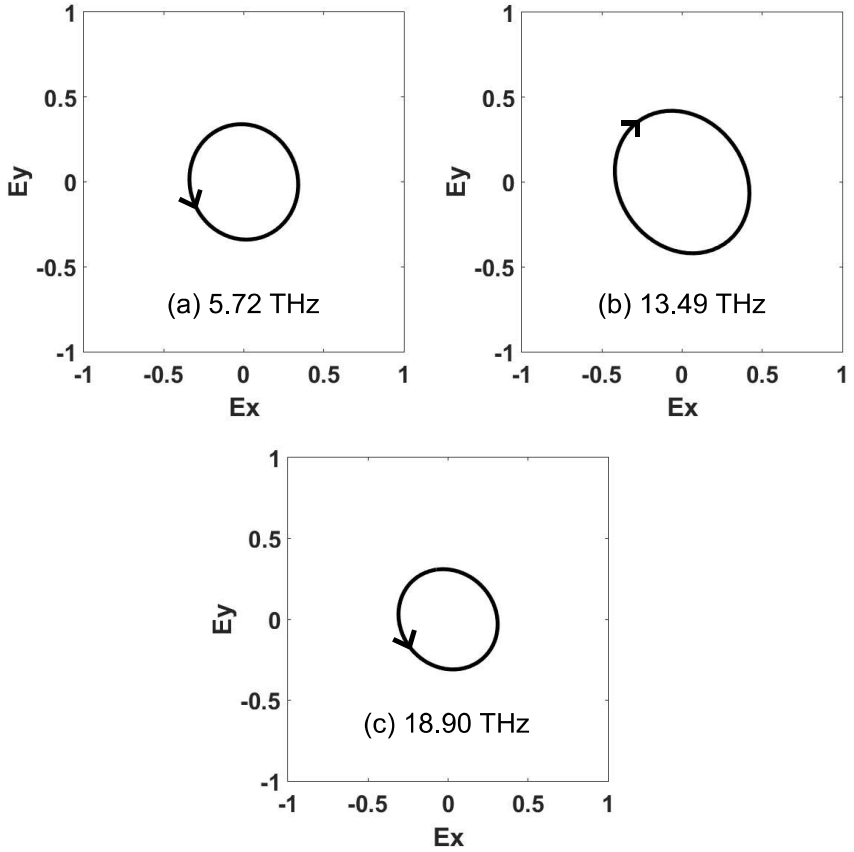

Fig. 4.24. Polarization ellipses formed at the transmitting end of the proposed TTLCPC at the above said three different frequencies (5.72 THz, 13.49 THz and 18.90 THz).

patch and the slotted metallic bottom layer [351]-[352]. It has been observed from Fig. 4.25(a) that the most optimized response has been achieved for $p_2 = 10$ μm. Thereafter, the AR response of the structure has been studied under variations of the periodicity (p_3) of the unit cell. The AR response undergoes blue-shift since the mutual coupling among the adjacent graphene patches gets decreased with an increase in the periodicity, as evident from Fig. 4.25(b) [353]. The best response has been achieved at $p_3 = 12$μm. The change in the thickness of SiO_2 substrate (t) leads to the variation in coupling strength between the top graphene patch and the bottom slotted-gold layer. With an increase in t, the enhancement of fringing electric field occurs resulting in the decrease of the frequency of polarization conversion as illustrated in Fig. 4.25(c) [243]. However, the increase of t makes the structure thicker, thereby defeating its purpose to be thin.

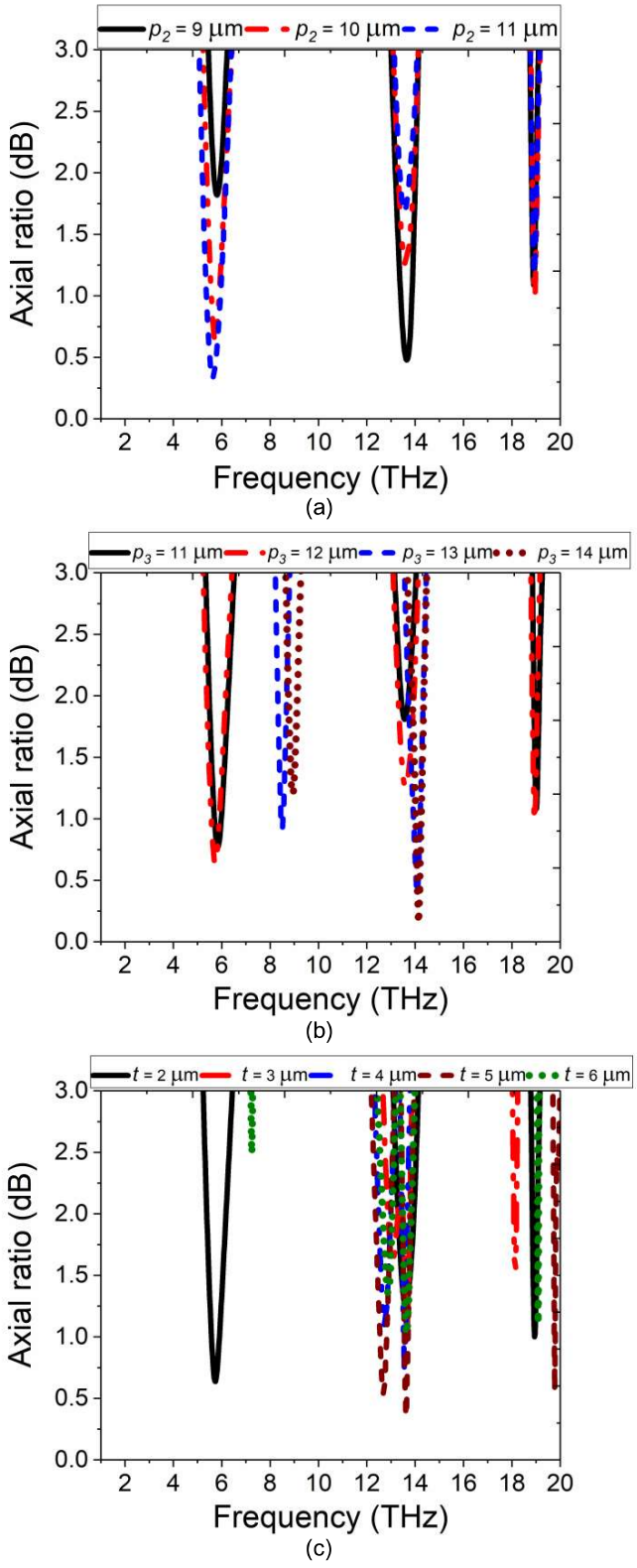

Fig. 4.25. Axial ratio performances of the proposed TTLCPC within the spectral range under (a). different graphene patch sizes (p_2), (b). the variation of the periodicity of the unit cell (p_3) and (c). the variation of the thickness of the substrate (t).

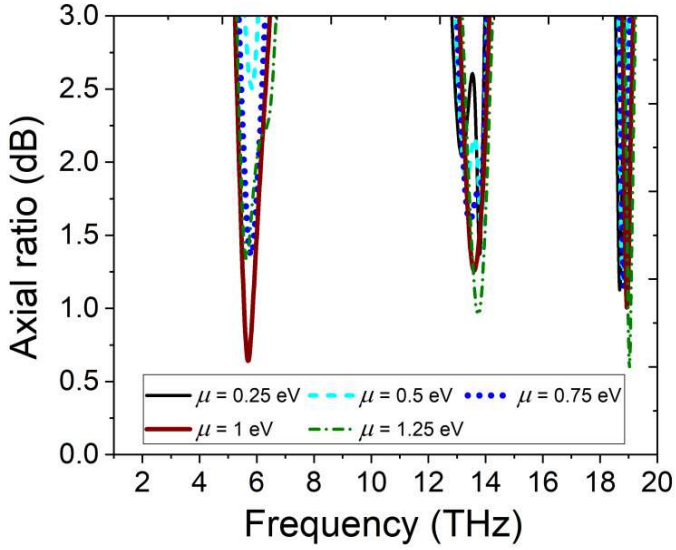

Fig. 4.26. Axial ratio (dB) versus frequency performance of the proposed TTLCPC under different chemical potential (μ) values of the graphene layer.

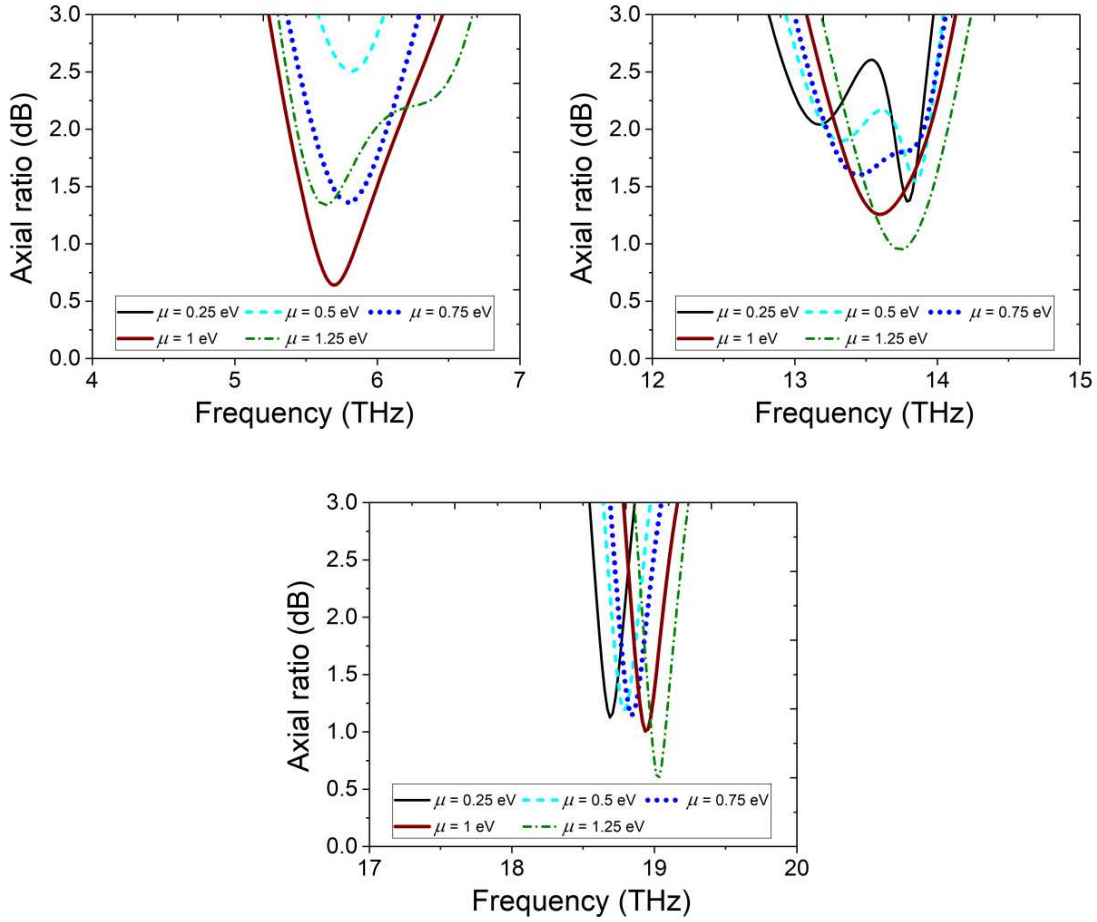

Fig. 4.27. Axial ratio (dB) variations at the individual frequency bands of the proposed TTLCPC under different chemical potential (μ) values of the graphene layer.

The chemical properties (μ) of the graphene patch have also been varied to check the performance of the spectral response of the AR. The change in chemical potential alters the surface conductivity as well as the impedance of the graphene, which further makes changes in the AR performance of the transmitted EM wave from the proposed TTLCPC. The difference in chemical potential (μ) of graphene offers the tunability of the AR response, as verified from Fig. 4.26. The individual response at the three distinct frequency bands under axial ratio variation has been depicted in Fig. 4.27. The proposed device has also been examined under different incident angles (θ) of the EM wave. It has been observed that there is a minute shift of AR response under variation of θ shown in Fig. 4.28. Circular polarization of the transmitted wave holds good till 40° incident angle, as observed from Fig. 4.28. The bottom layer consists of perpendicularly oriented two U-shaped slots which produces triple band circular polarization (CP) conversion of linearly polarized (LP) EM wave as mentioned in Fig. 4.29.

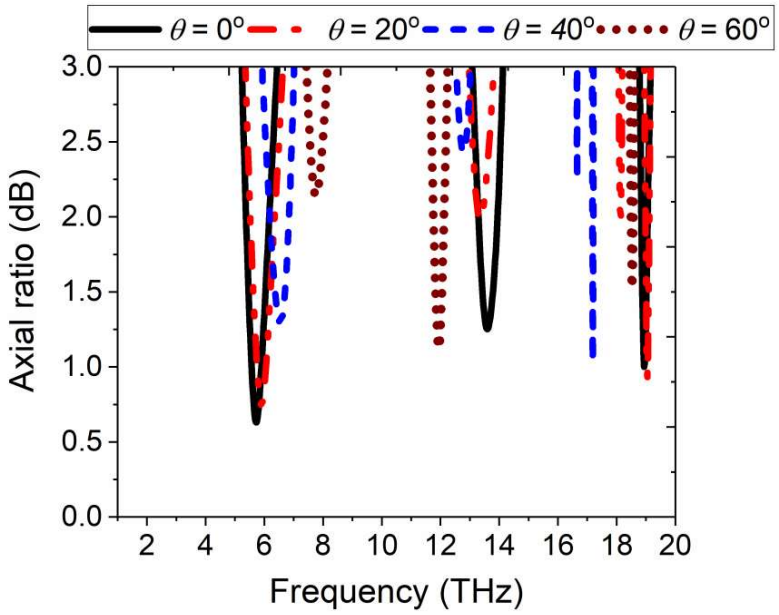

Fig. 4.28. Axial ratio (dB) versus frequency performance of the proposed TTLCPC under different incident angles (θ) of the wave.

The backside slot on the gold layer of the proposed device has been optimized employing different steps to achieve the desired response. First, the smaller U-shaped slot has been

designed to get a single transmission band at 18.94 THz with circular polarization. The corresponding axial ratio (AR) response along with the E-field pattern on the bottom gold surface and U-shaped slotted bottom gold layer has been shown in Fig. 4.30.

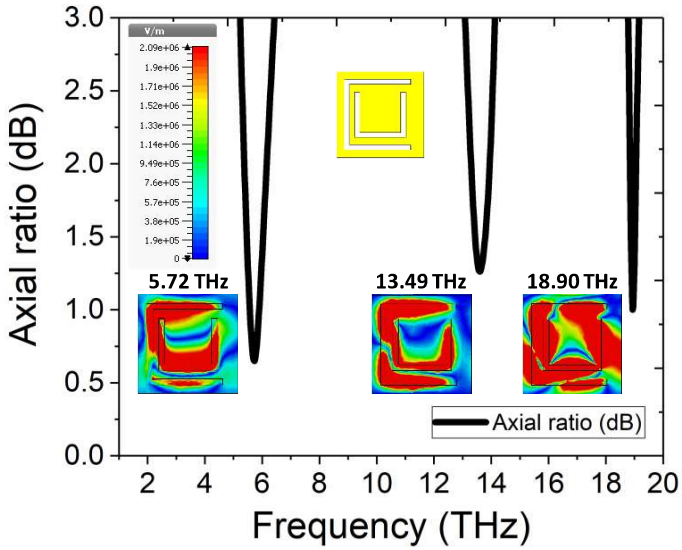

Fig. 4.29. Frequency response of the proposed TTLCPC at 5.72 THz, 13.49 THz and 18.90 THz when both slots are present on the backside gold layer of the proposed TTLCPC.

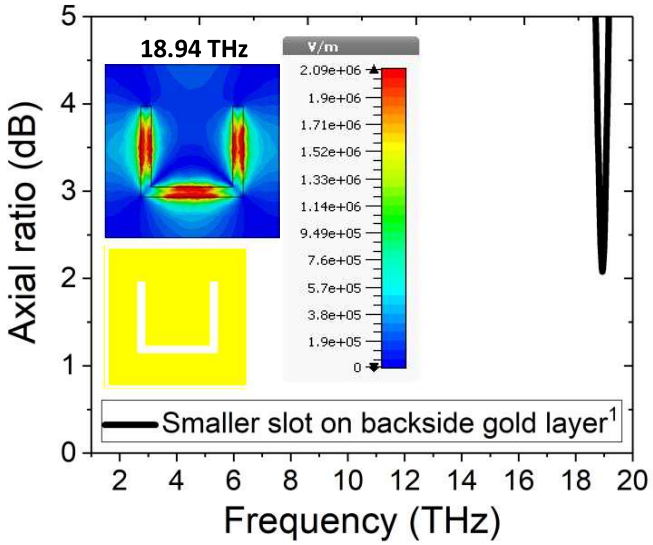

Fig. 4.30. Frequency response of the proposed TTLCPC at 18.94 THz when only smaller slot with first configuration is present on the backside gold layer.

Next, the same slot has been clockwise rotated by 90°. It can be observed that the AR is less than 3 dB at 18.93 THz, as observed from Fig. 4.31. The E-field pattern at the same frequency has been studied in Fig. 4.31 too. Thereafter, the U-shaped slot has been made larger to achieve

AR dips at 13.67 THz and 18.82 THz. The corresponding E-field patterns have been depicted in Fig. 4.32(a), and Fig. 4.32(b).

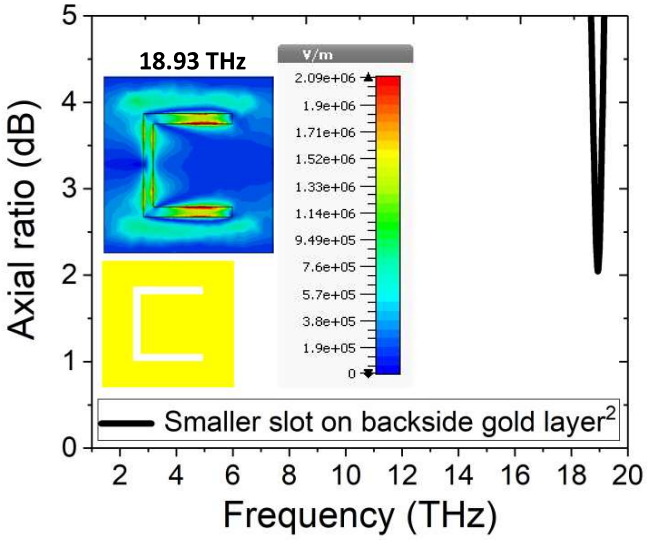

Fig. 4.31. Frequency response of the proposed TTLCPC at 18.93 THz when only smaller slot with second configuration is present on the backside gold layer.

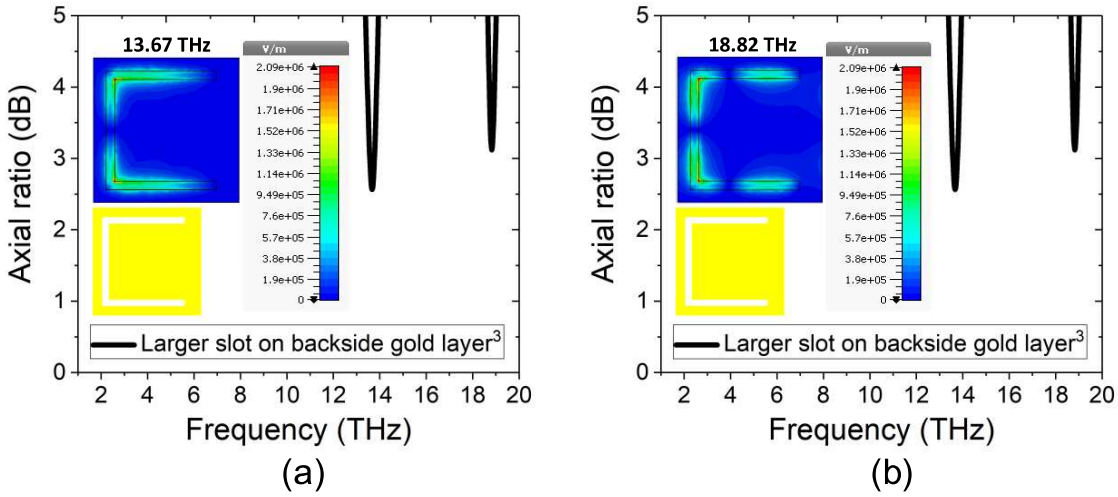

Fig. 4.32. Frequency response of the proposed TTLCPC when only larger slot is present on the backside gold layer (a) at 13.67 THz and (b) at 18.82 THz, respectively.

A further 90° clockwise rotation of the U-slot on the bottom metallic layer has been incorporated to achieve circular polarizations at 13.67 THz, and 18.82 THz. The E-field pattern corresponding to the aforementioned frequencies are depicted in Fig. 4.33(a) and Fig. 4.33(b).

Now, the AR responses have been studied with the presence of both the slots where three axial ratio dips with improved performance of circular polarization have been achieved at 5.72 THz, 13.49 THz and 18.90 THz, respectively. The E-field patterns at these frequencies are illustrated

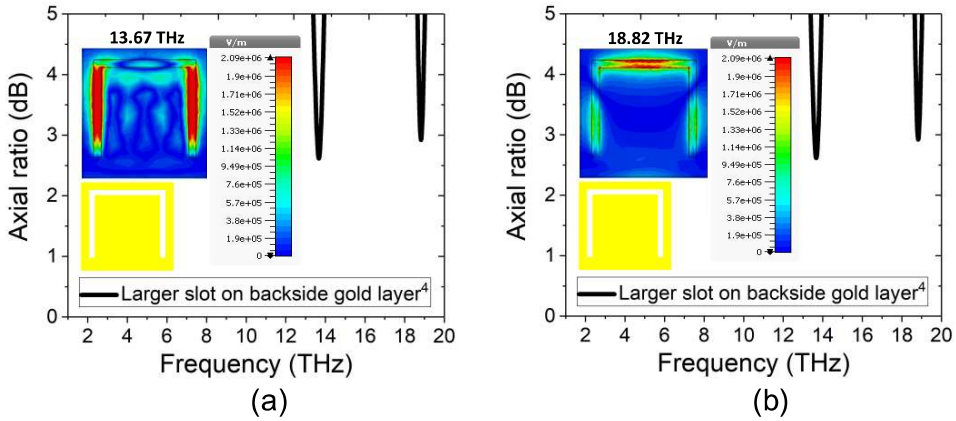

Fig. 4.33. Frequency responses of the proposed TTLCPC when 90° clockwise rotated larger slot is present on the backside gold layer (a) at 13.67 THz and (b) at 18.82 THz, respectively.

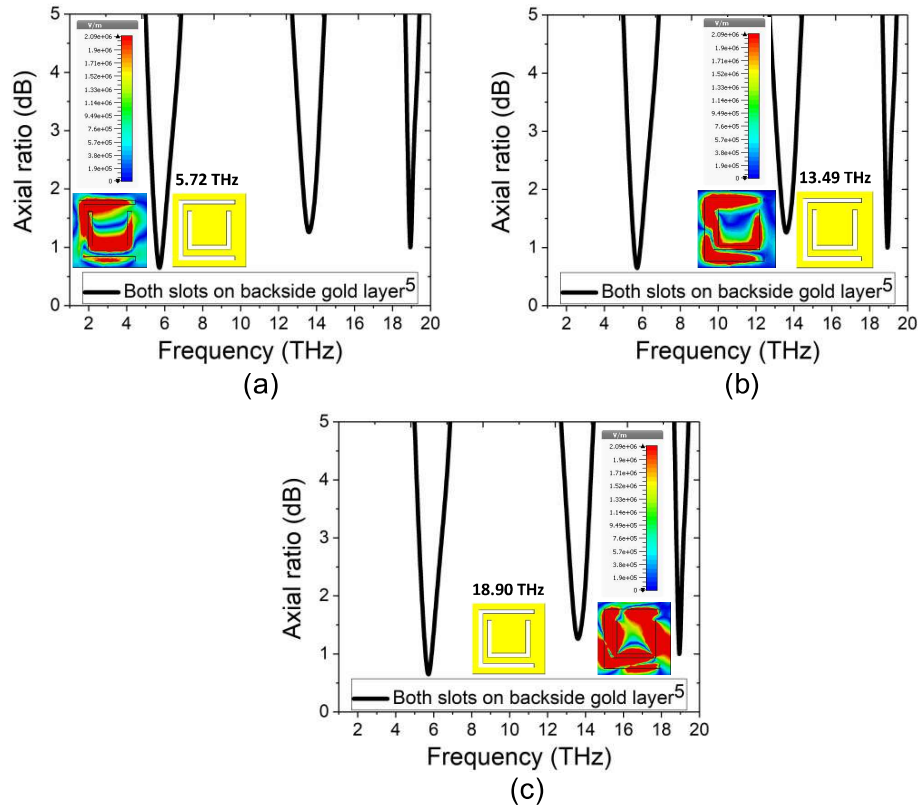

Fig. 4.34. Frequency responses of the proposed TTLCPC when both slots are present on the backside gold layer (a) at 5.72 THz (b) at 13.49 THz and (c) at 18.90 THz, respectively.

Table 4.4. Comparison With Existing Graphene-Based LP to CP Converters

Graphene-based LTCPCs	**Frequency range (THz)**	**Size of lattice (approx.)**	**Thickness (approx.)**	**Angular stability (θ°)**
S. Wu, D. Zha, Y. He, L. Miao and J. Jiang [354]	Single band 3.8 THz	λ/6.39	λ/1.5	60°
T. Guo and C. Argyropoulos [355]	Single band 4.75 THz	λ/8	λ/42	Only at 45°
Proposed device	Tripple band (5.72 THz, 13.49 THz and 18.90 THz)	λ/4.35	λ/26.11	40°

in Fig. 4.34(a), Fig 4.34(b) and Fig. 4.34(c) respectively. The smaller slot on the bottom gold surface generates one single AR dip while the larger one on the bottom gold surface produces two AR dips. In the optimization process, both the slots are merged together with different orientation configurations and simultaneously checked. It can be seen from Table 4.4 that to date the linear to circular polarization conversion has been achieved at a single frequency band only employing graphene-based metasurface design [33, 34]. On the other hand, the proposed design shows linear to circular polarization conversion incorporating graphene-based metasurface design at three distinct frequency bands of 5.72 THz, 13.49 THz and 18.90 THz.

4.9 Conclusions

In conclusion, we demonstrate a simpler configuration of a graphene-based metasurface for linear to circular polarization conversion where all the essential features have been enhanced than the existing terahertz counterparts (refer to Table I). The device can find highly promising and unique characteristics for futuristic applications as it stipulates a wideband LP to CP conversion of 2.25 THz in the ‘Terahertz Gap’. The Stokes’ parameters have been calculated for the verification of LP to CP conversion of the EM wave. Further, the CP nature of the reflected wave has been validated by constructing polarization ellipses at the operating

frequency band while varying the chemical potential (μ) of the graphene metasurface to validate the tunable nature of the proposed RLCPC. A detailed circuit model has been introduced for the support of the EM simulated outputs of the proposed RLCPC. The device provides stable operation till 40° incident angles in terms of polarization conversion bandwidth, as depicted from the spectral response of the AR. This RLCPC would have immense potential usefulness in THz beam scanning antennas, RCS reduction, and THz antennas for easy switching of polarization states between uplinking and downlinking for space applications, military radar applications, etc.

Next, a graphene-based transmittive-type linear to circular polarization converter (TTLCPC) at three frequency bands in the lower MIR range covering the terahertz gap has been presented in the later-half of the chapter. Stokes' coefficients have been evaluated to calculate the ellipticity (e) and axial ratio (dB) in the desired spectral bands for the verification of the transmitted EM wave to be a circularly polarized one at those three spectral bands. The polarization ellipses generated at 5.72 THz, 13.49 THz and 18.90 THz depicts the orientations of the circular nature of the transmitted electromagnetic wave such as left-handed circular polarization (LHCP) and right-handed circular polarization (RHCP) of the transmitted wave. The device offers stable CP nature of the transmitted wave till 40° incident angles of the EM wave. The proposed device is ultra-thin having a thickness of $\lambda/26.11$ and compact in nature by maintaining a periodicity of $\lambda/4.35$ with respect to the lowest frequency band. This TTLCPC can be useful for THz communication, THz detection, THz sensing and THz imaging etc. It also can be applied directly to the planar linearly polarized antennas to have circular polarization of EM wave at the desired frequency bands.